WASHINGTON UNIVERSITY
DEPARTMENT OF PHYSICS
LABORATORY FOR ULTRASONICS
St. Louis, Missouri 63130

"Ultrasonic Nondestructive Evaluation Techniques Applied to the Quantitative Characterization of Textile Composite Materials"

Semiannual Progress Report: December 12, 1996 - June 12, 1997

NASA Grant Number: NAG 1-1848

Principal Investigator:

Dr. James G. Miller
Professor of Physics

The NASA Technical Officer for this grant is:

Dr. William P. Winfree
NASA Langley Research Center
Hampton, Virginia

Ultrasonic Nondestructive Evaluation Techniques Applied to the Quantitative Characterization of Textile Composite Materials

I. Introduction

In this Progress Report, we describe our further development of advanced ultrasonic nondestructive evaluation methods applied to the characterization of anisotropic materials. We present images obtained from experimental measurements of ultrasonic diffraction patterns transmitted through water only and transmitted through water and a thin woven composite. All images of diffraction patterns have been included on the accompanying CD-ROM in the JPEG format and Adobe™ Portable Document Format (PDF), in addition to the inclusion of hardcopies of the images contained in this report.

In our previous semi-annual Progress Report (NAG 1-1848, December, 1996)[1], we proposed a simple model to simulate the effect of a thin woven composite on an insonifying ultrasonic pressure field. This initial approach provided an avenue to begin development of a robust measurement method for nondestructive evaluation of anisotropic materials. In this Progress Report, we extend that work by performing experimental measurements on a single layer of a five-harness biaxial woven composite to investigate how a thin, yet architecturally complex, material interacts with the insonifying ultrasonic field.

In Section II of this Progress Report we describe the experimental arrangement and methods for data acquisition of the ultrasonic diffraction patterns upon transmission through a thin woven composite. We also briefly describe the thin composite specimen investigated. Section III details the analysis of the experimental data followed by the experimental results in Section IV. Finally, a discussion of the observations and conclusions is found in Section V.

II. Experimental Arrangement and Methods

All measurements in this study were performed in an immersion tank using a set of 0.5" diameter, spherically-focused (4" focal length), piezoelectric transducers with nominal center frequencies of 5 MHz, 10 MHz, and 15 MHz (Panametrics V309, V311, and V319, respectively) as the transmitting transducer. For notational purposes, we refer to the different transducers by their nominal center frequency (i.e., the 5 MHz transmitting transducer). The thin woven composite was positioned in the focal plane of the transmitting transducer and oriented normal to the beam axis of the transducer. The thin composite, as mentioned above, is a single layer (less than 1 mm thick) of a five-harness biaxial weave. A 1 mm diameter PVDF, broadband, needle hydrophone (Force Institute, Type MH28-10) was used as the receiving transducer. The receiving hydrophone was positioned 120 mm from the transmitting transducer (approximately 20 mm from the back side of the specimen). In the receiving plane, the hydrophone sampled the ultrasonic pressure field in a two-dimensional pseudo-array manner[2]. The pseudo-array was composed of 64 sites by 64 sites (4096 total sites) with 0.5 mm separation between adjacent sites for a total sampled area of 31.5 mm by 31.5 mm.

Figure 1 is a schematic diagram showing the data acquisition system used in this investigation. The transmitting transducer was excited with a broadband pulse generated by a Panametrics 5800 pulser/receiver. The ultrasonic signal received by the hydrophone was initially sent through a unity-gain preamplifier (Force Institute, Type BAS) matched specifically to the hydrophone, providing 50 Ω coupling to the receive-side electronic equipment. The signal was then sent through a pair of programmable attenuators (HP 8494G and 8496G) that permitted precise adjustment of the signal amplitude to prevent saturation of the input stage of the receiving electronic equipment and to maximize the dynamic range of the oscilloscope. From the attenuators, the received signal went to the receiving stage of the Panametrics 5800 pulser/receiver, and finally on to a Tektronix 2430 digital oscilloscope for digitization. An Apple Macintosh IIfx computer

utilized in-house custom software written in the C programming language to acquire the rf time traces and store them for off-line analysis.

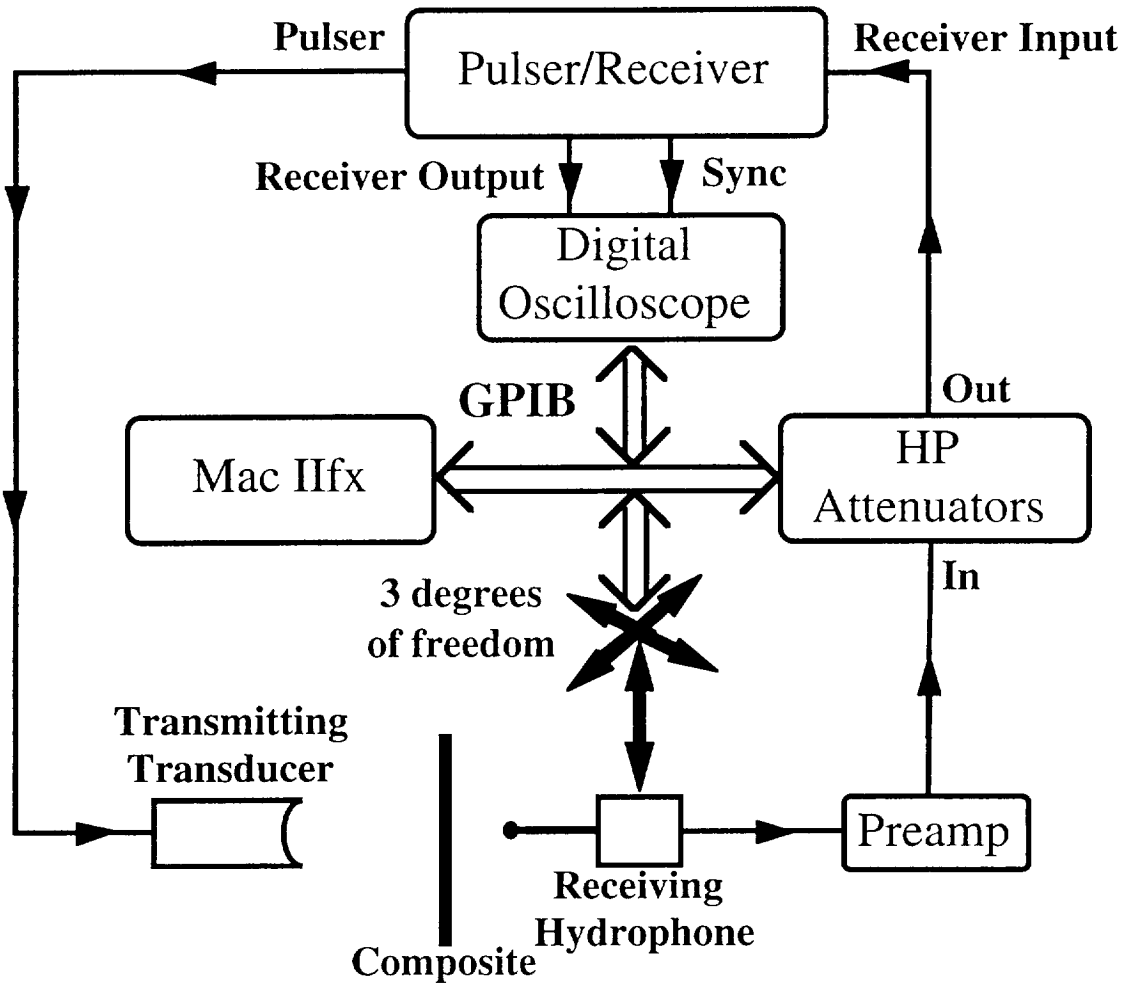

Figure 1: Experimental Setup.

It is a goal of this ongoing experimental research to understand how systematic variations of the acquisition system, as well as changes in the materials investigated, affect the quantitative evaluation of these materials. The first physical parameter we chose to vary systematically was the nominal center frequency of the transmitting transducer. Three transmitting transducers were employed for the acquisition of the experimental data discussed within this report.

Prior to pseudo-array scanning of the ultrasonic beam through the thin composite, dynamic range measurements of the experimental system with the thin composite inserted were performed for each transmitting transducer. At the origin of the pseudo-array, a series of rf traces were acquired with the insertion of a range of attenuations (0 dB to 60 dB in 5 dB steps). At each attenuation setting, 64 rf time traces were acquired and averaged off-line before being stored to disk. The voltage scale of the digital oscilloscope was adjusted in order to maximize the dynamic range of the oscilloscope. Each rf time trace acquired throughout this study consisted of 1024 points sampled in the interleave mode at 250 MegaSamples/s (0.004 μs sampling period). (The stability of the rf time trace at all sites insured there would be no averaging problems with the oscilloscope operating in the interleave mode.) The digital oscilloscope was externally triggered by a synchronization pulse provided by the Panametrics 5800. The data acquisition delay time (relative to the trigger signal) was set manually such that the received trace was localized within the acquisition window.

Following the measurement of the dynamic range of the experimental system with the thin composite inserted, the transmitted beam through the thin composite was scanned in a pseudo-array manner, as described above. In addition to maximizing the dynamic range of the oscilloscope at the pseudo-array origin site, the programmable attenuators were adjusted to maximize the dynamic range of the receive-side electronics. At each site of the pseudo-array, 64 rf time traces were acquired and averaged off-line before being stored to disk.

To investigate how the spatial variation of the weave pattern for the thin woven composite affects the phase fronts of the ultrasonic signal, we conducted four pseudo-array scans with each transducer. Figure 2 illustrates the relative positioning of the four different scan regions with respect to the thin composite. The center of each pseudo-array scan was linearly separated by 3 mm from the previous pseudo-array scan. These four regions provide a fair representation of the different types of regions that would be encountered in subsequent studies of this thin composite.

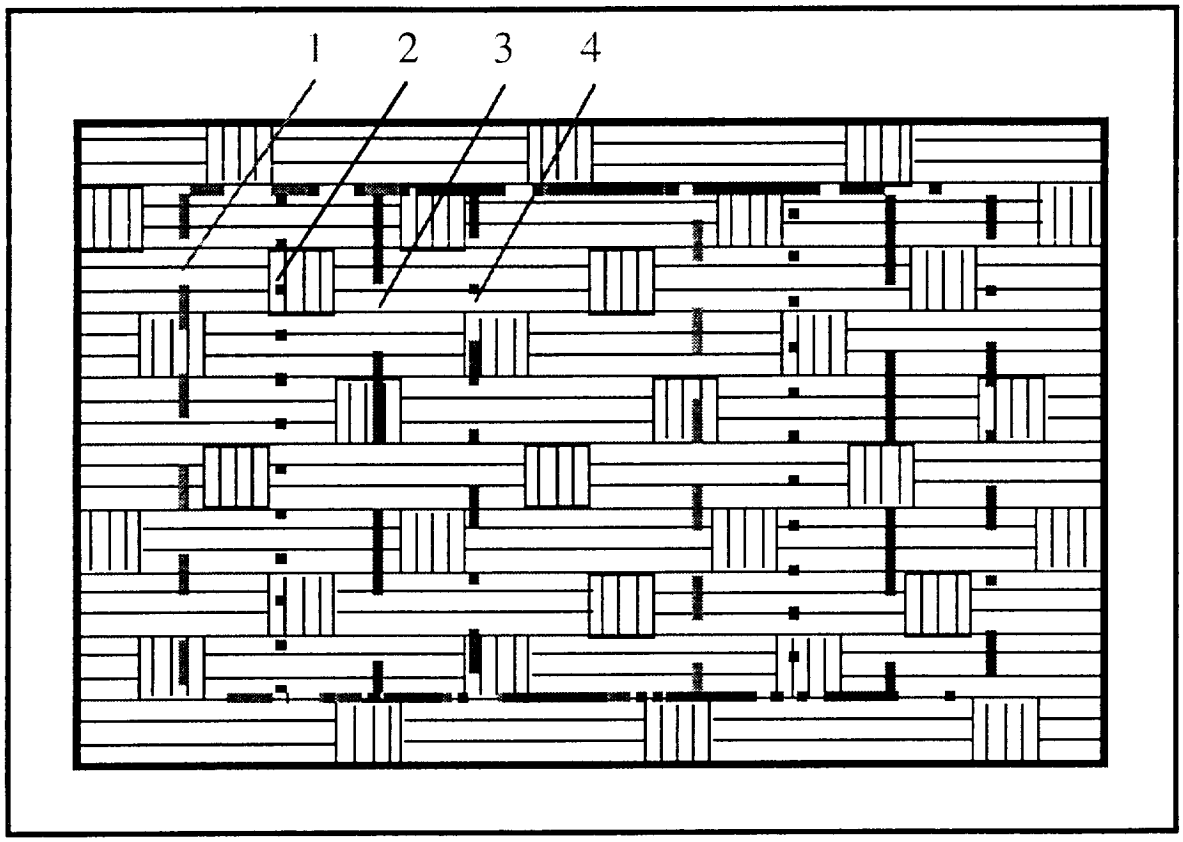

Figure 2: Relative positioning of different scanned regions of the thin woven composite.

III. Data Analysis

Software

Data analyses and visualization were performed on a Power Macintosh using in-house custom software written in the C programming language, in conjunction with a commercial graphing package (DeltaGraph® Pro 3.5, DeltaPoint, Inc., Monterey, CA) and an imaging software package (Transform 3.3, Fortner Research LLC, Sterling, VA).

Dynamic Range Measurement Analysis

For the dynamic range measurements, each averaged rf time trace was Fast Fourier Transformed. The magnitude of the Fast Fourier Transform was then squared to provide the power spectrum. In addition, for each transducer, the differences in power spectra were calculated by subtracting the power spectrum resulting from the insertion of 10 dB of attenuation from each

power spectrum. The dynamic range power spectra and relative power spectra for each transmitting transducer were then plotted.

Pseudo-Array Measurement Analysis

For the pseudo-array scans, the time-averaged rf trace acquired at each pseudo-array site was Fast Fourier Transformed and the magnitude of the Fast Fourier Transform was calculated. To provide a more robust approach for material evaluation, we performed a narrowband averaging analysis on the data. Discrete frequency data within a 1 MHz bandwidth was extracted from the broadband pressure magnitude spectra, and subsequently averaged to provide a narrowband magnitude representation of the measured pressure field. The 1 MHz bandwidth typically corresponded to 5 or 6 data points, dependent upon where the 1 MHz bandwidth fell on the discretely sampled pressure magnitude spectrum. Averaging over frequencies offered the advantage of reducing susceptibility to unrepresentative single frequency events (outliers).

For each of the three transmitting transducers, we acquired five sets of data (one water path and four composite paths). For each data set, narrowband analysis was performed over three distinct frequency ranges (see Table 1). For the 5 MHz transmitting transducer, we calculated narrowband magnitudes of the pressure field for 2.5 MHz to 3.5 MHz, 4.5 MHz to 5.5 MHz, and 6.5 MHz to 7.5 MHz. For the 10 MHz transmitting transducer, we calculated narrowband magnitudes of the pressure field for 7.5 MHz to 8.5 MHz, 9.5 MHz to 10.5 MHz, and 11.5 MHz to 12.5 MHz. Finally, for the 15 MHz transmitting transducer, we calculated the narrowband magnitudes of the pressure field for 10.5 MHz to 11.5 MHz, 12.5 MHz to 13.5 MHz, and 14.5 MHz to 15.5 MHz.

Magnitude Image Construction

Image construction of the experimentally measured narrowband magnitude of the ultrasonic pressure field was performed using Transform 3.3. For all images, only the central region (central 32 sites by 32 sites, i.e., 15.5 mm by 15.5 mm) of the pseudo array appears. Cropping the

images permitted zooming the region where effects due to changes in physical parameters (i.e., water path versus composite path, insonifying frequency, and composite position) were most significant. All magnitude of the pressure field images are presented using grayscale mappings. Darker regions correspond to larger relative pressure magnitudes and lighter regions correspond to smaller relative pressure magnitudes. For purposes of presentation, the images were interpolated to present smooth transitions across the receiving pseudo-array aperture. A bilinear interpolation method (row then column) calculates the grayscale for each pixel of the image.

Transducer	Narrowband Ranges
5 MHz	2.5 MHz to 3.5 MHz
	4.5 MHz to 5.5 MHz
	6.5 MHz to 7.5 MHz
10 MHz	7.5 MHz to 8.5 MHz
	9.5 MHz to 10.5 MHz
	11.5 MHz to 12.5 MHz
15 MHz	10.5 MHz to 11.5 MHz
	12.5 MHz to 13.5 MHz
	14.5 MHz to 15.5 MHz

Table 1: Narrowband ranges for the transducers.

Figure 3 shows a representative pressure magnitude field overlaid with a cartoon of the composite weave pattern. It also provides relevant dimensions for the images.

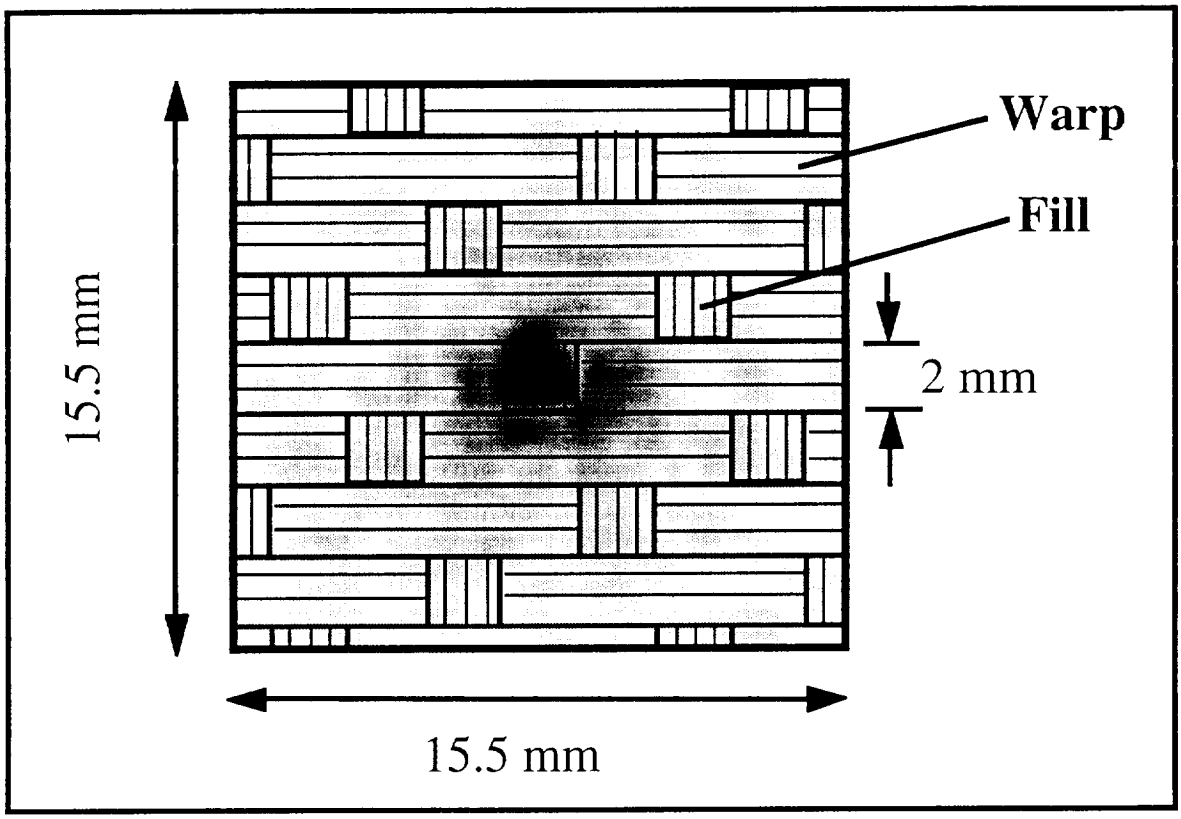

Figure 3: Representative pressure magnitude image with a cartoon of the thin woven composite overlaid.

For each series of scans (1 water path and 4 composite paths) for a particular transmitting transducer, a set of images was constructed (3 sets total) consisting of 3 sections. All the images of this report employ grayscale mapping. However, within each section, images are displayed using a data floor and data ceiling specific to that section to calculate the bin size. Therefore, the same data ranges are mapped to the same gray value for the images within each section (i.e., bin sizes are the same). The use of this grayscale mapping technique permits direct comparison of images *within* each image section. We do not provide direct comparison for images from different transducers because system effects have not been completely deconvolved for the use of different transducers. However, we can still make some general observations between these sets as will be discussed later.

The first section of an image set compares pressure magnitude measurements for water path only to pressure magnitude measurements with the thin composite inserted. The second section

compares magnitude measurements from different scanned regions of the thin woven composite for a particular narrowband frequency. The third and final section of an image set for a given transducer compares the pressure magnitudes for a given thin composite position at different insonifying frequencies. Table 2 provides the organization to the sets of the images constructed.

IV. Results

In this Section we discuss the dynamic range measurement results and the receiver plane images of the experimentally measured narrowband magnitude of the pressure field through water path only and through the thin woven composite. Please see either the hardcopy images included with this report or the accompanying CD-ROM for viewing of images discussed in this Section.

Figures 4, 6, and 8 show representative power spectra for the 5 MHz, 10 MHz, and 15 MHz transmitting transducers, respectively, for different electronic attenuation settings with the thin composite inserted in the signal path. Figures 5, 7, and 9 show representative difference power spectra (with respect to the power spectrum obtained for 10 dB of attenuation) for the 5 MHz, 10 MHz, and 15 MHz transmitting transducers, respectively. The vertical dashed lines in each figure demarcate the 10 dB-down region for the power spectrum. These figures provide confidence that all experimental data acquired for this report were within the usable bandwidth of the acquisition system, in addition to being well above the noise floor and below the saturation ceiling.

Table 2 offers an index to the figures of the images constructed. As described above, each of the 3 sets are organized into 3 sections (see Chart 1). Each set is composed of 10 figures. The first section of each set consists of three pairs of images: the narrowband magnitudes for water path and composite path at three narrowband ranges. The second section has three subsections of four images: the narrowband magnitudes of the four different composite positions at three narrowband ranges. The third section of each set has four subsections of three images: the narrowband magnitudes for the three narrowband ranges at the four composite positions.

Figures	Transducer	Description
10 to 12	5 MHz	Compare water path to composite path
13 to 15		Compare different composite positions
16 to 19		Compare different frequencies
20 to 22	10 MHz	Compare water path to composite path
23 to 25		Compare different composite positions
26 to 29		Compare different frequencies
30 to 32	15 MHz	Compare water path to composite path
33 to 35		Compare different composite positions
36 to 39		Compare different frequencies

Table 2: Pressure magnitude image figures.

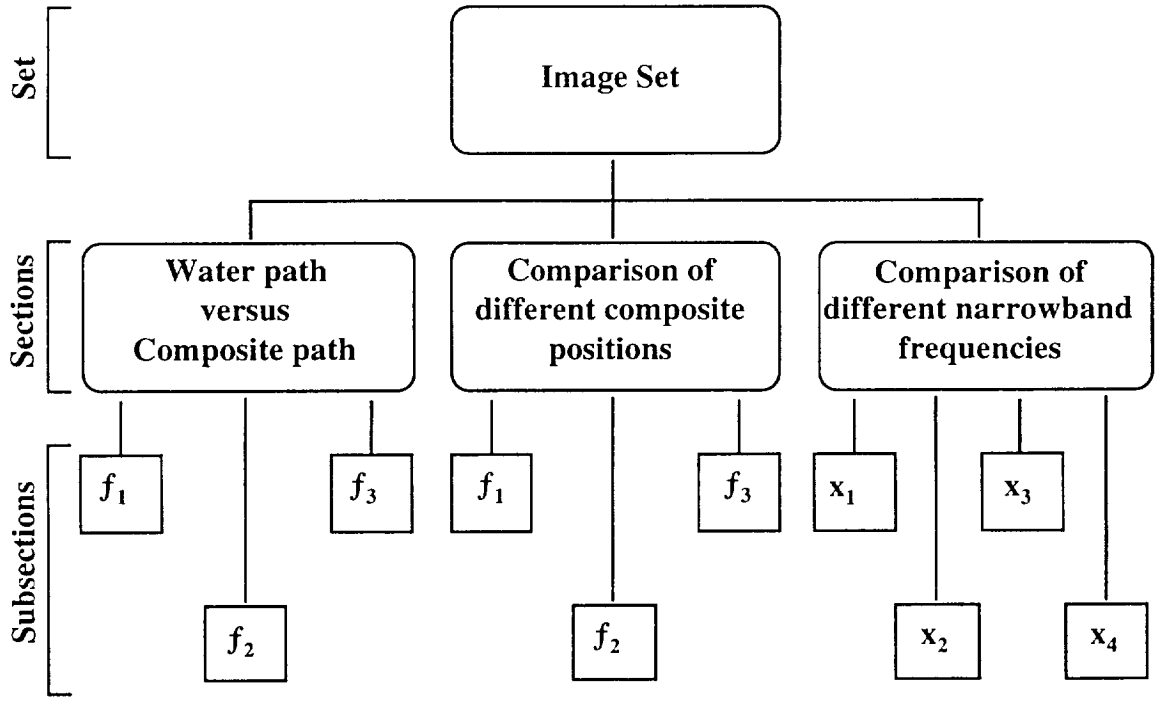

Chart 1: Organizational chart of an image set. Each image set is divided into 3 sections. The f's represent the narrowband frequency ranges and the x's represent the composite positions.

V. Discussion

A) *Comparison of Water Path versus Thin Composite Path*

Inspection of the images comparing the pressure magnitude for water path and composite path provides several general observations (see Figures 10 to 12, 20 to 22, 30 to 32). First, there is an apparent decrease in pressure magnitude for the ultrasonic signal which passes through the thin composite. This decrease is expected due to the reflection losses at the water-composite interfaces, in addition to the attenuation encountered from propagation through the thin composite as compared to water path only. Second, the disruption of the circular symmetry of the ultrasonic beam due to the insertion of the composite is evident. A contribution to the observed loss of symmetry of the ultrasonic pressure magnitude may be due to a very slight non-normal incidence of the ultrasonic beam with respect to the fill orientation of the thin composite (see Figure 40)[3,4]. As the ultrasonic beam interrogates different regions of the thin woven composite, the fill orientation with respect to the ultrasonic beam will change. It is this anisotropy of the fill orientation with respect to axis of the ultrasonic beam that can contribute to the distortion of the ultrasonic beam, and, in turn produce a mottled and distorted pressure magnitude field[5]. In addition, there will be a wavelength dependence to the interaction of the ultrasonic field with the fill. We could imagine that another thin composite of a different weave pattern would result in a different distortion of the ultrasonic signal. For both the water paths and the composite paths it is apparent that as frequency increases (wavelength decreases) the cross-sectional area of the ultrasonic beam decreases, thus decreasing the area (volume) of insonification. This is discussed further in the following subsection.

B) *Comparison of Insonifying Frequencies*

As we increase the frequency of insonification, the diameter of our ultrasonic beam decreases (see Figures 16 to 19, 26 to 29, and 36 to 39). This decrease in the ultrasonic

beam diameter, most notable for the higher frequencies, is of importance when the main beam diameter is on the order of or smaller than features of the composite (i.e., the fiber bundle size). In this case, the pressure magnitude images can be highly dependent upon the region of the composite insonified and the wavelength of the insonifying beam. For instance, the ultrasonic beam diameter could be contained within one fiber bundle or it may overlay the edge of a fiber bundle (see Figure 41). These two situations can produce distinctly different results.

For frequencies of 10 MHz and greater we are able to view the finer details of the thin composite, such as the fiber bundle size. Rough measurements from the images show the fiber bundle dimensions to be approximately 2 mm which agrees well with measurement of the fiber bundle size of the thin composite.

Knowledge of the insonifying volume as a function of frequency becomes increasingly important if one wishes to extend these observations to the use of true two-dimensional transmitting and receiving arrays. With available digital technologies, dynamic focusing of a two-dimensional array will permit customized focusing of the ultrasonic field.

C) *Comparison of Thin Composite Positions*

At lower frequencies (longer wavelengths), the main beam diameter is large enough that on average approximately the same type of region is insonified (see Figures 13 to 15). This reduces the amount of pressure magnitude variation that we observe between the different composite regions for a given frequency. In contrast, as mentioned above, the pressure magnitude images for the different scanned regions are more sensitive at higher frequencies (see Figures 23 to 25 and 33 to 35).

References

1. James G. Miller, "Ultrasonic Nondestructive Evaluation Techniques Applied to Quantitative Characterization of Textile Composite Materials", NASA, Progress Report, Report Number: NAG 1-1848, (December, 1996).

2. Mark R. Holland and J.G. Miller, "Phase-Insensitive and Phase-Sensitive Quantitative Imaging of Scattered Ultrasound Using a Two-Dimensional Pseudo-Array", 1989, (Chicago, Published 1988), Vol. 88 CH 2578-3, pp. 815-819.

3. Brian N. Cox and Gerry Flanagan, "Handbook of Analytical Methods for Textile Composites", NASA, Report Number: Contractor Report 4750, (March, 1997).

4. K.K. Shung and J.M. Dzierzanowski, "Effects of Phase-Cancellation on Scattering Measurements", *Ultrasonic Imaging*, Vol. 4, pp. 56-70, (1982).

5. Peter W. Marcus and Edwin L. Carstensen, "Problems with Absorption Measurements of Inhomogeneous Solids", *J. Acoust. Soc. Am.*, Vol. 58, pp. 1334-1335, (1975).

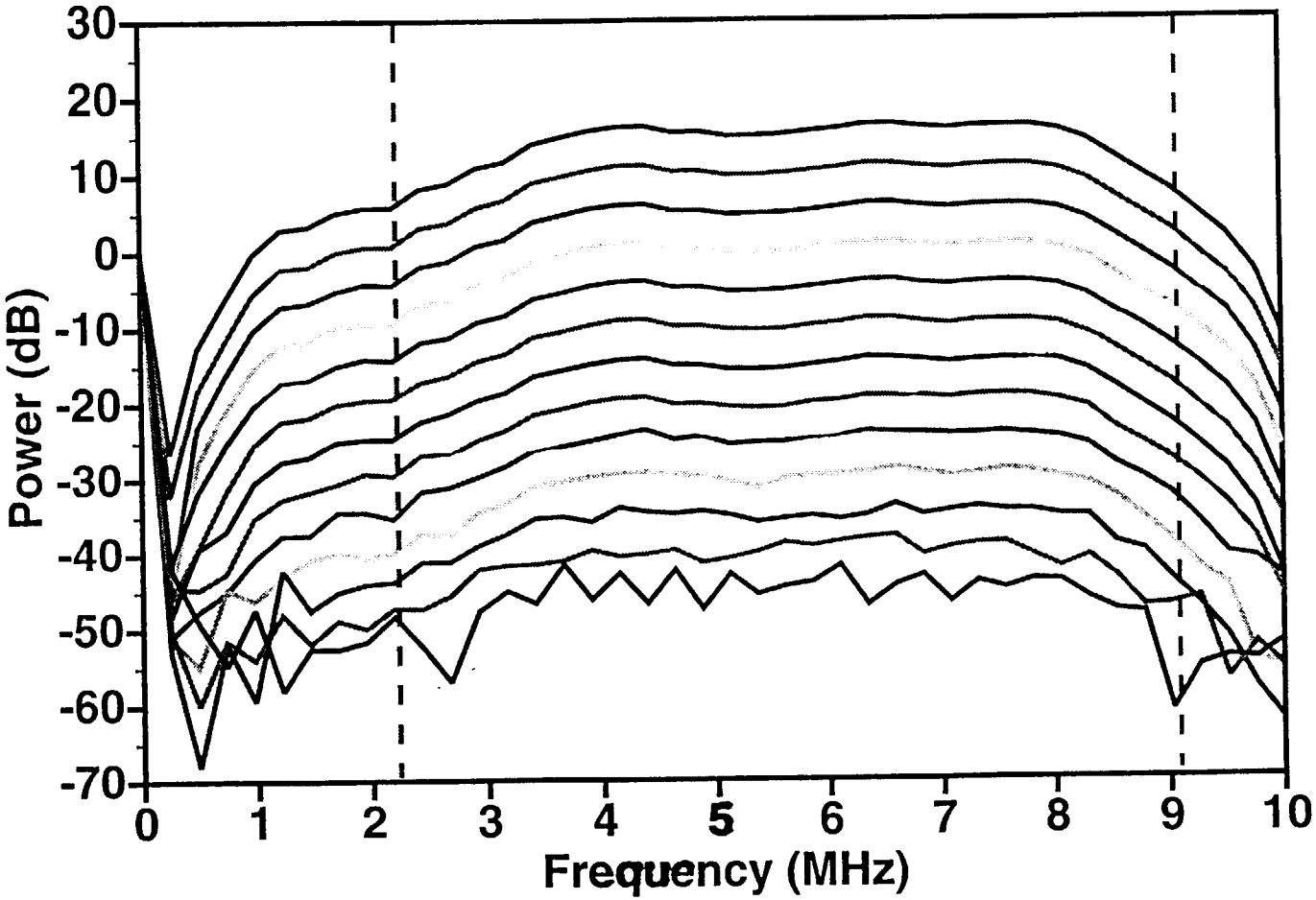

Figure 4: Power spectra of the thin woven composite for the 5 MHz transmitting transducer resulting from the insertion of attenuation in 5 dB steps. The vertical dashed lines demarcate the 10 dB-down region ($\approx$ 2 to 9 MHz).

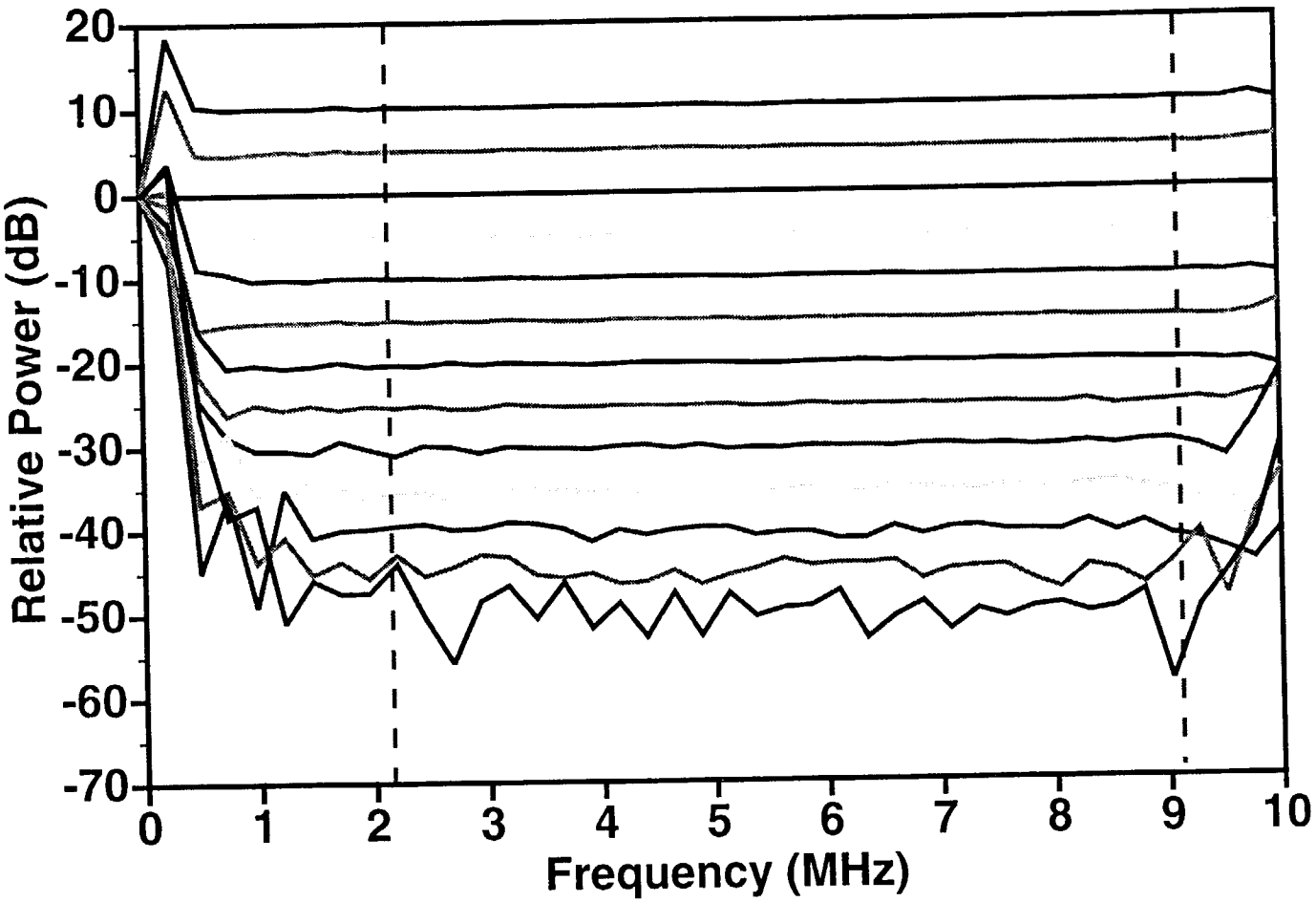

Figure 5: Relative power spectra of the thin woven composite for 5 MHz transmitting transducer resulting from the insertion of attenuation in 5 dB steps. The vertical dashed lines demarcate the 10 dB-down region ($\approx$ 2 to 9 MHz).

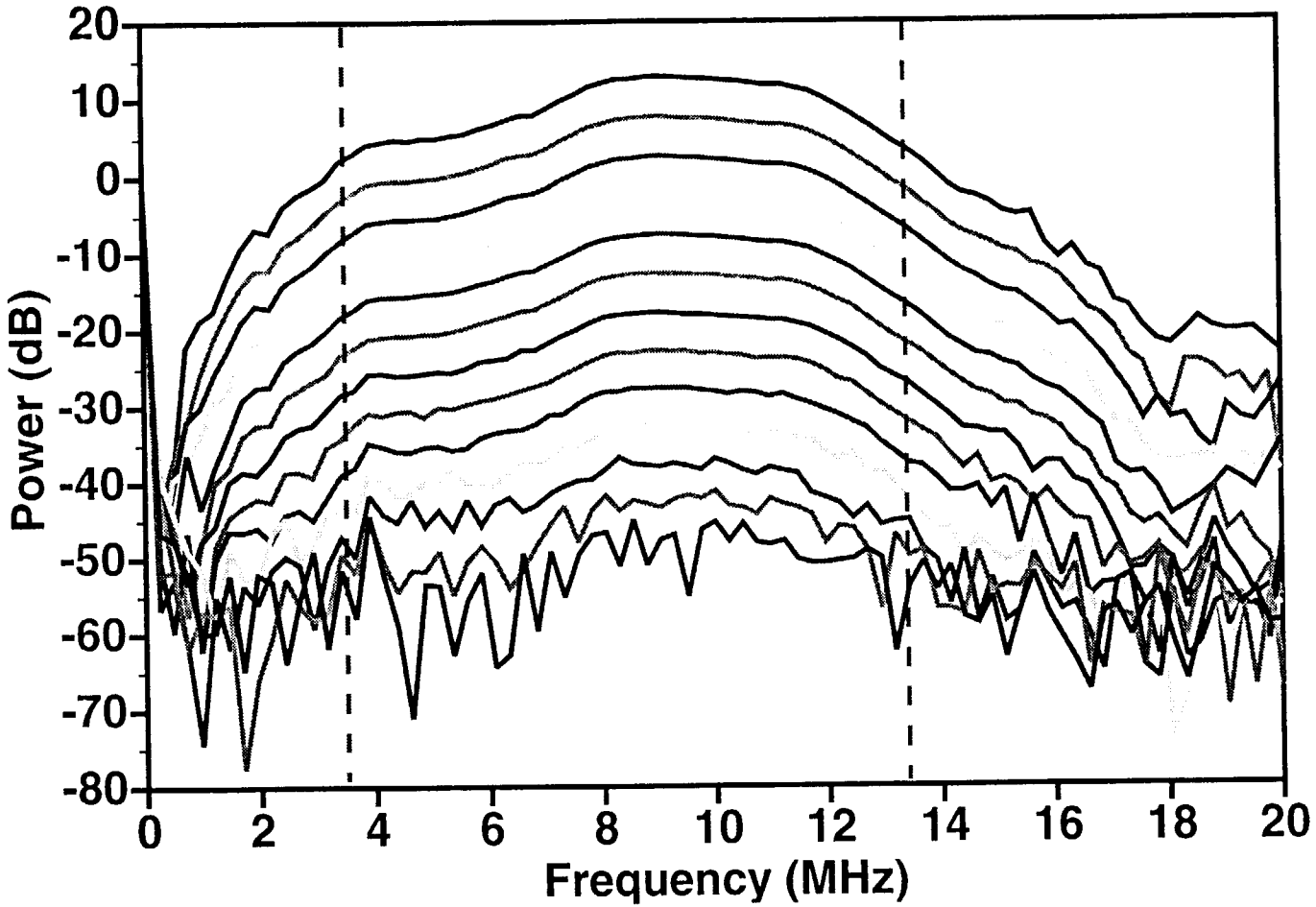

Figure 6: Power spectra of the thin woven composite for the 10 MHz transmitting transducer resulting from the insertion of attenuation in 5 dB steps. The vertical dashed lines demarcate the 10 dB-down region ($\approx$ 3.5 to 13.5 MHz).

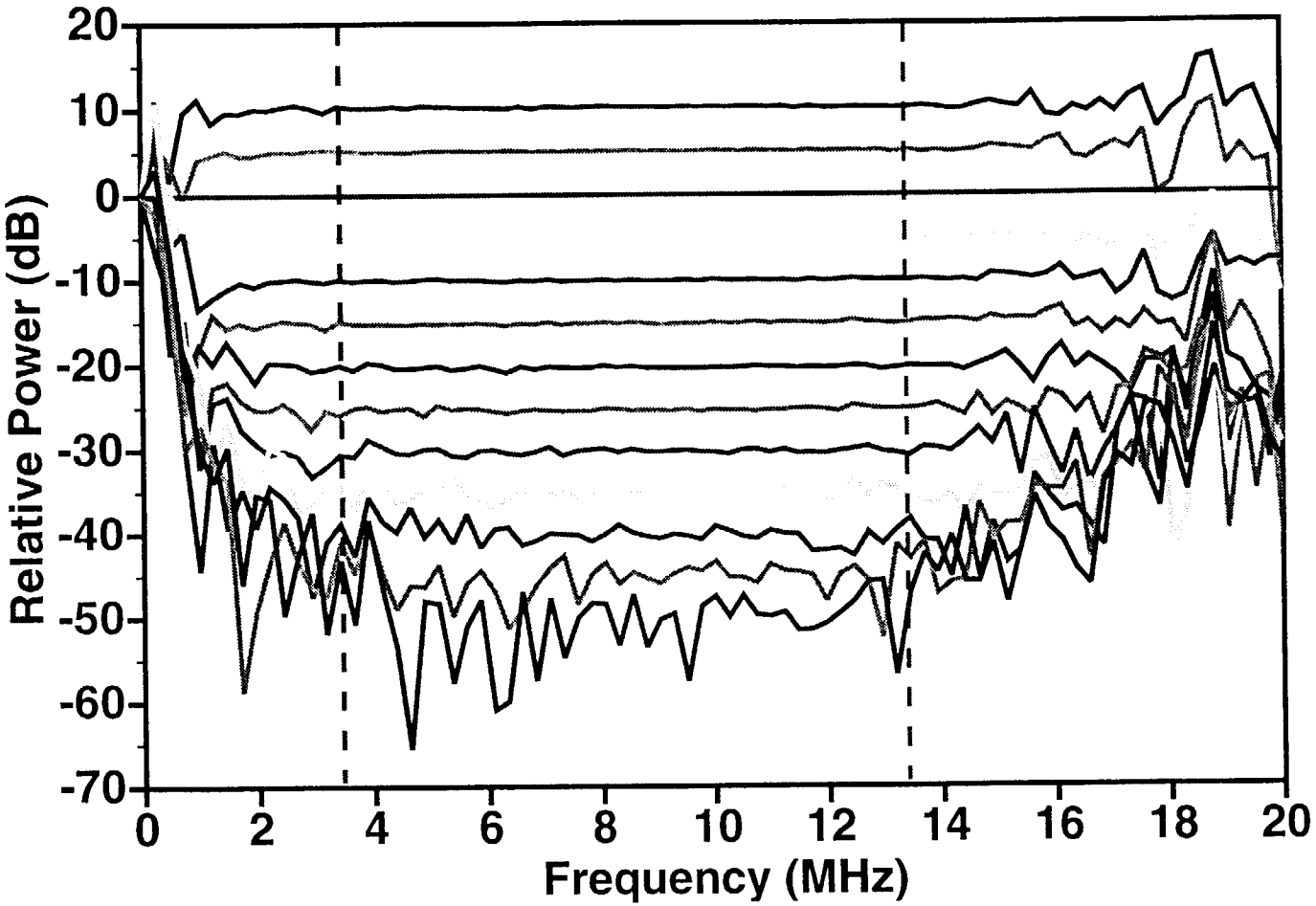

Figure 7: Relative power spectra of the thin woven composite for 10 MHz transmitting transducer resulting from the insertion of attenuation in 5 dB steps. The vertical dashed lines demarcate the 10 dB-down region ($\approx$ 3.5 to 13.5 MHz).

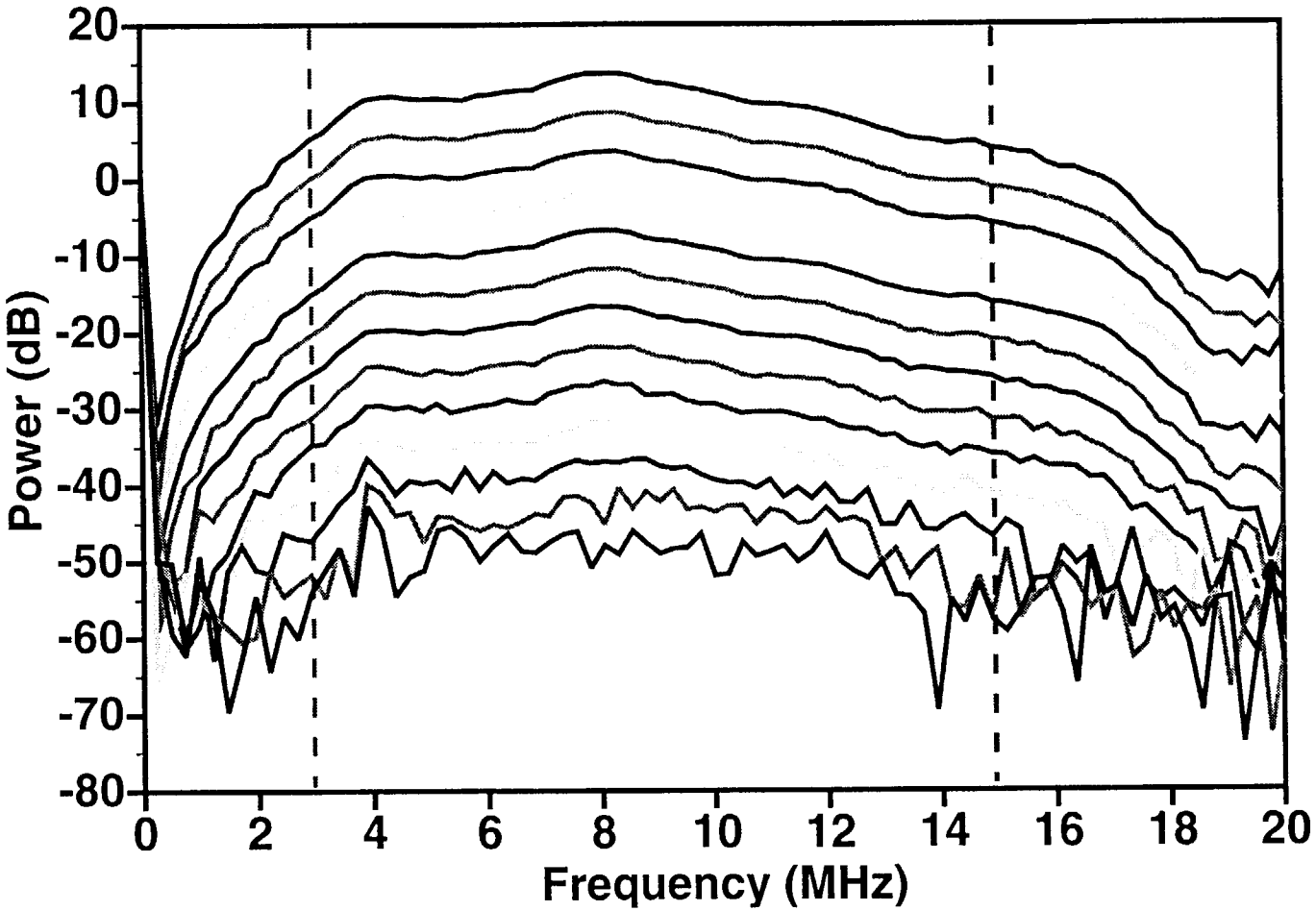

Figure 8: Power spectra of the thin woven composite for the 15 MHz transmitting transducer resulting from the insertion of attenuation in 5 dB steps. The vertical dashed lines demarcate the 10 dB-down region ($\approx$ 3 to 15 MHz).

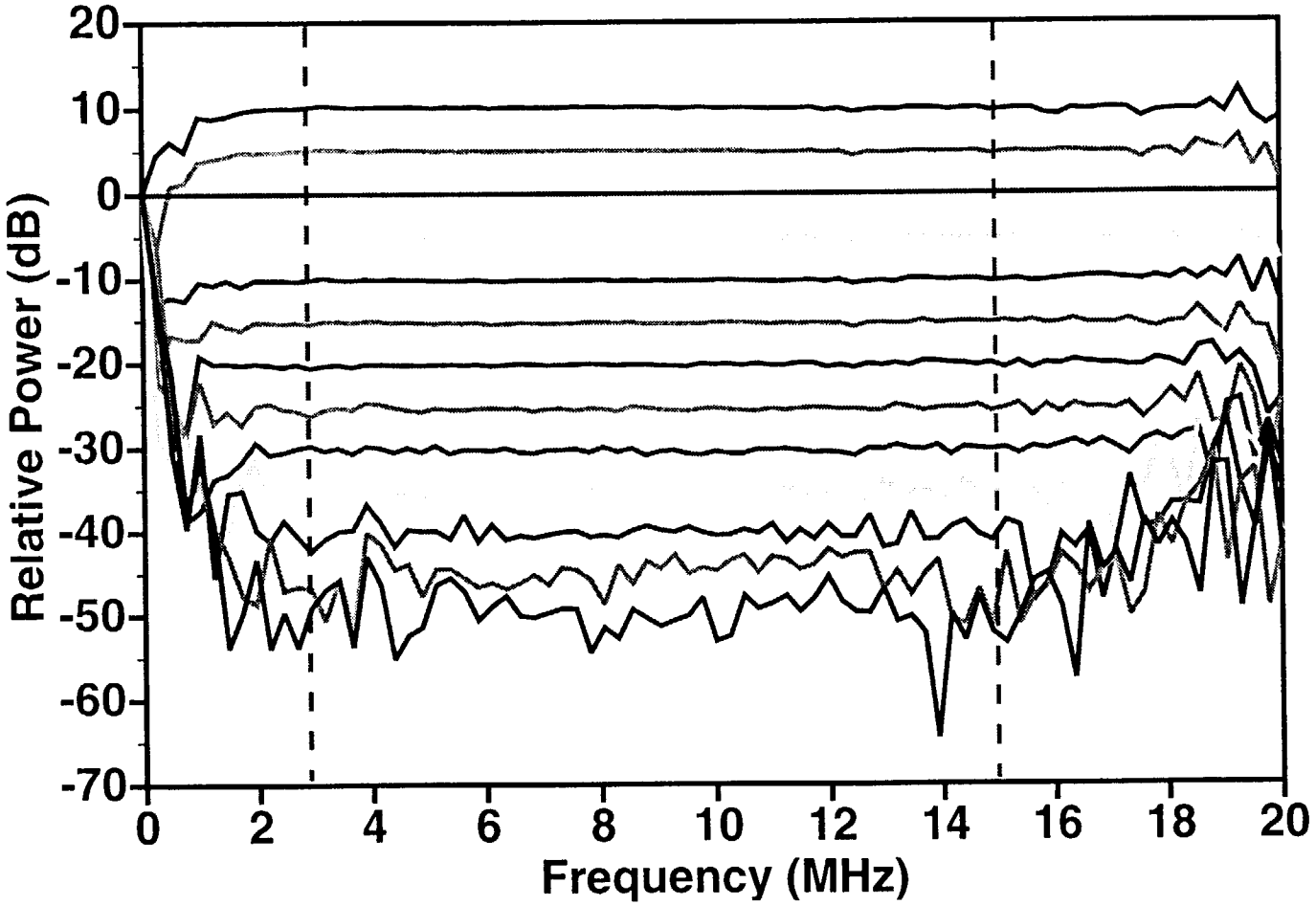

Figure 9: Relative power spectra of the thin woven composite for 15 MHz transmitting transducer resulting from the insertion of attenuation in 5 dB steps. The vertical dashed lines demarcate the 10 dB-down region (≈3 to 15 MHz).

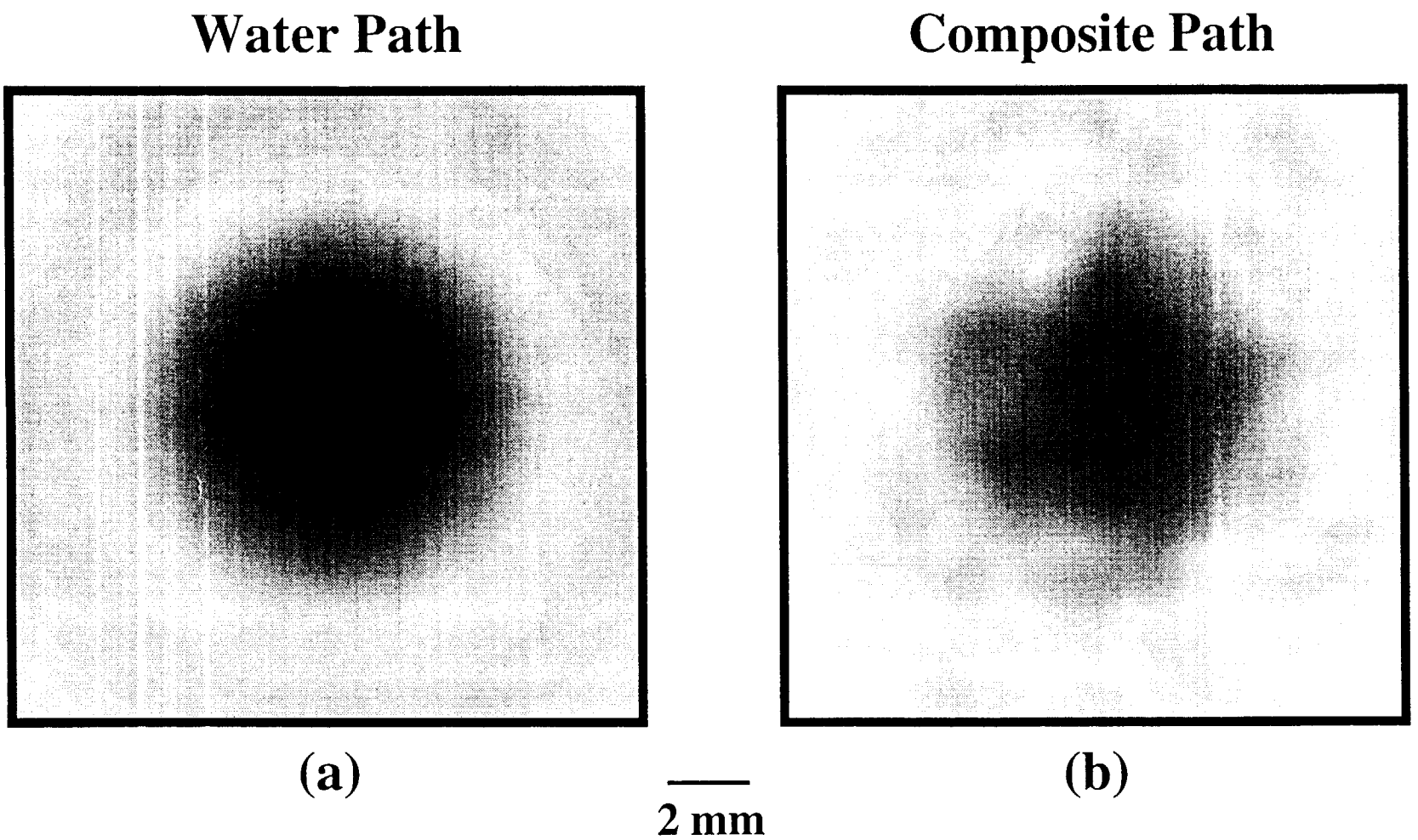

Figure 10: Water path versus composite path for 2.5 MHz to 3.5 MHz. Receiver plane images for (a) narrowband pressure magnitude for water path only and (b) narrowband pressure magnitude for composite path using the 5 MHz transducer.

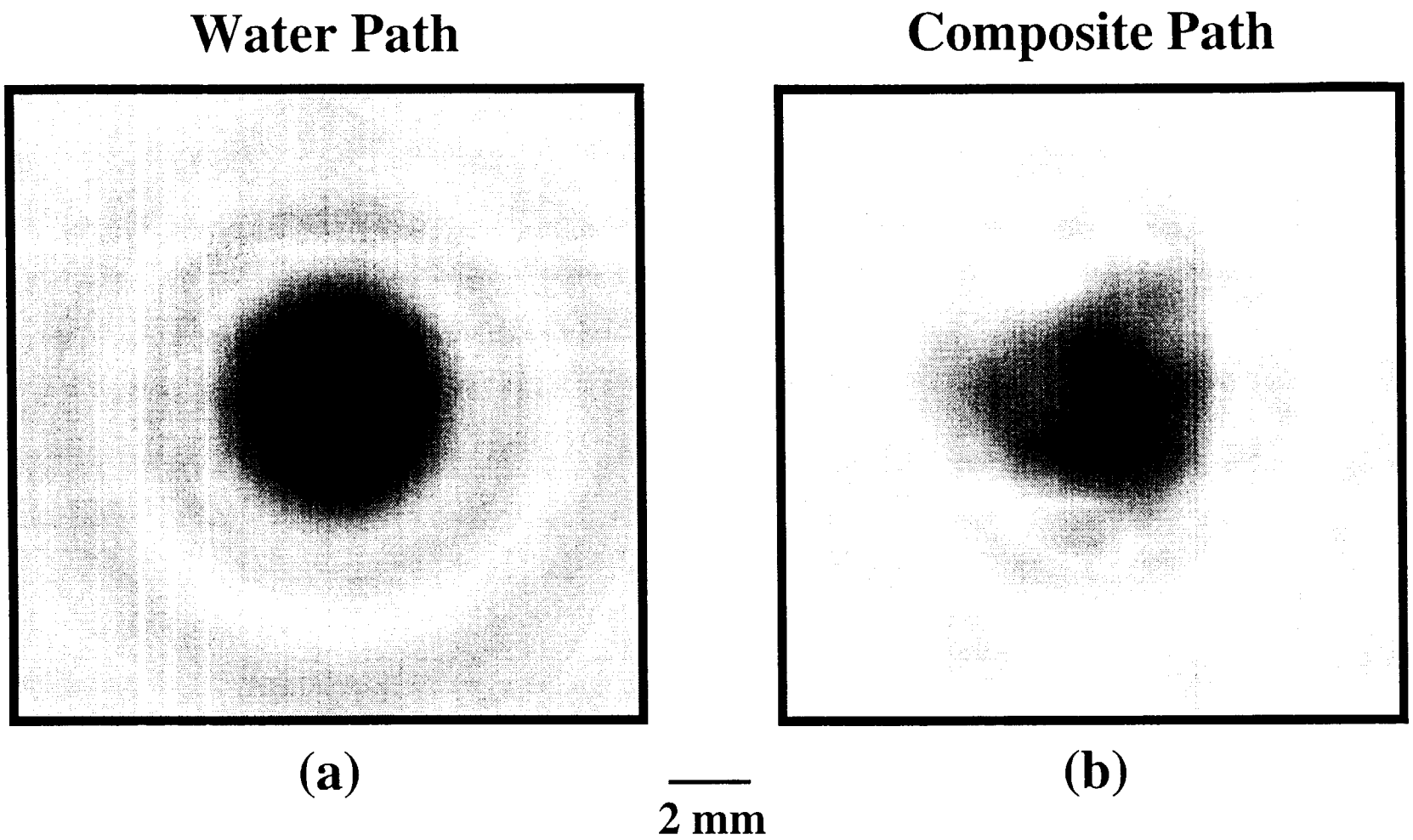

Figure 11: Water path versus composite path for 4.5 MHz to 5.5 MHz. Receiver plane images for (a) narrowband pressure magnitude for water path only and (b) narrowband pressure magnitude for composite path using the 5 MHz transducer.

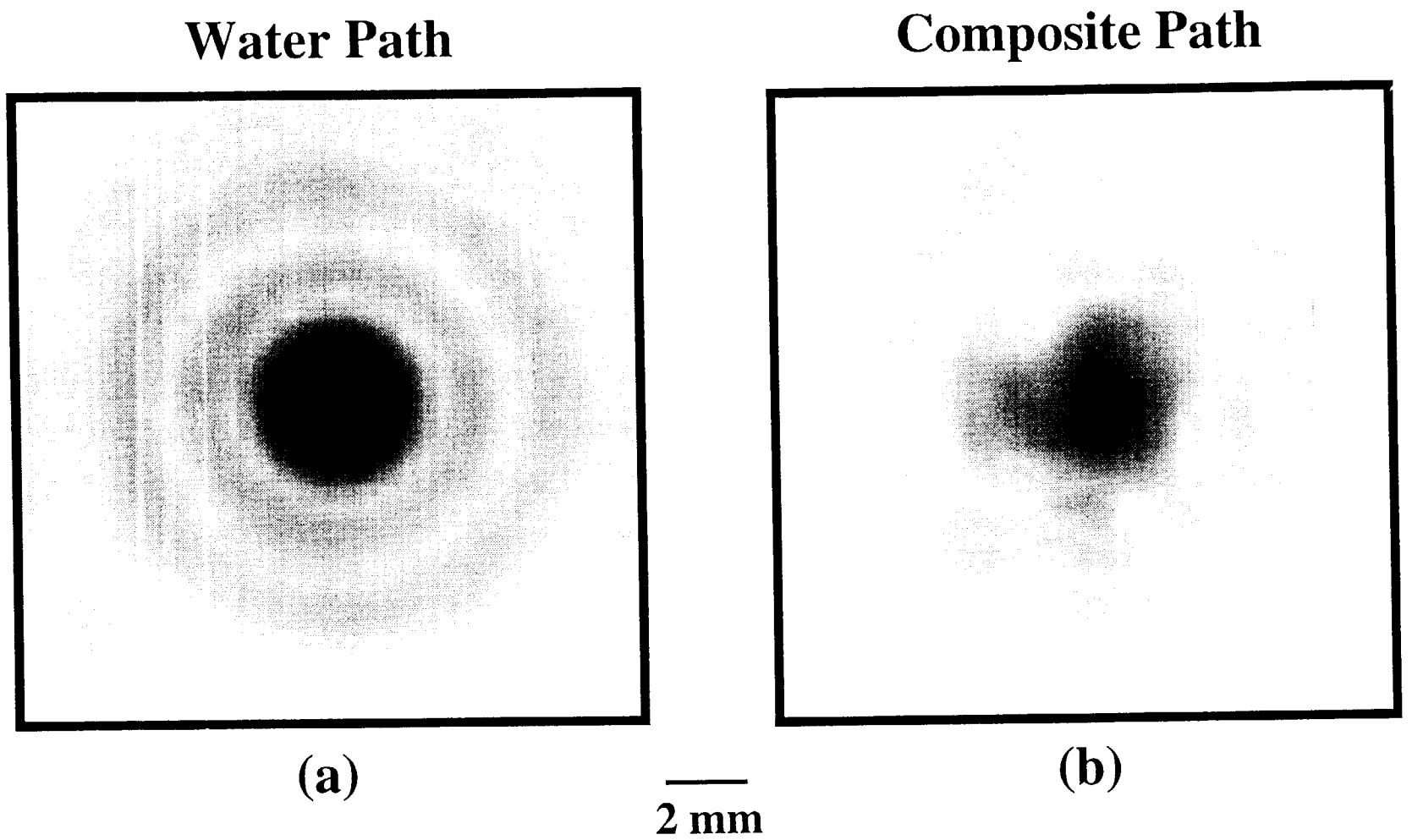

Figure 12: Water path versus composite path for 6.5 MHz to 7.5 MHz. Receiver plane images for (a) narrowband pressure magnitude for water path only and (b) narrowband pressure magnitude for composite path using the 5 MHz transducer.

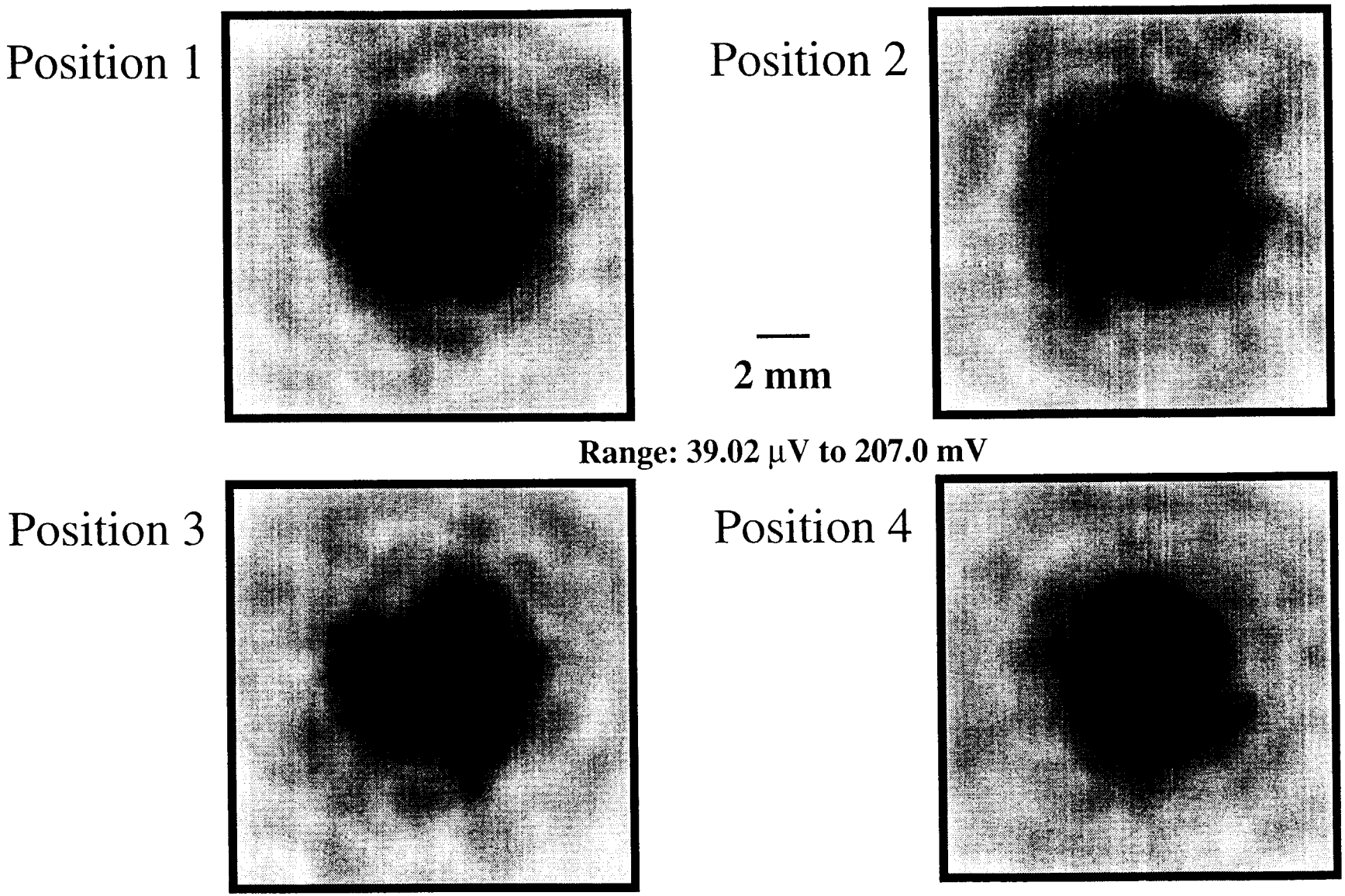

Figure 13: Comparison of positions for 2.5 MHz to 3.5 MHz. Receiver plane images of the narrowband pressure magnitude are shown for the different scanned regions of the thin composite using the 5 MHz transducer.

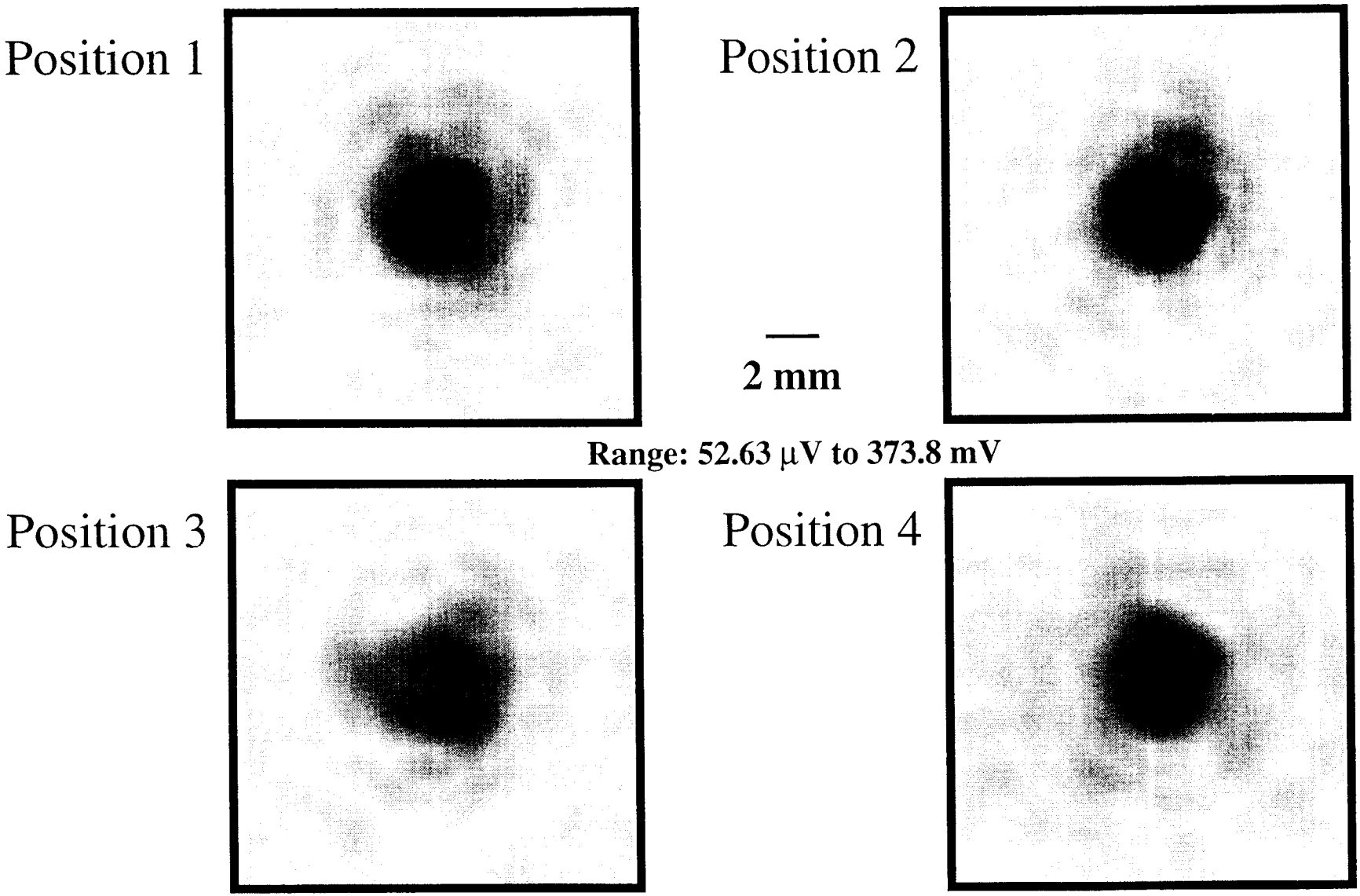

Figure 14: Comparison of positions for 4.5 MHz to 5.5 MHz. Receiver plane images of the narrowband pressure magnitude are shown for the different scanned regions of the thin composite using the 5 MHz transducer.

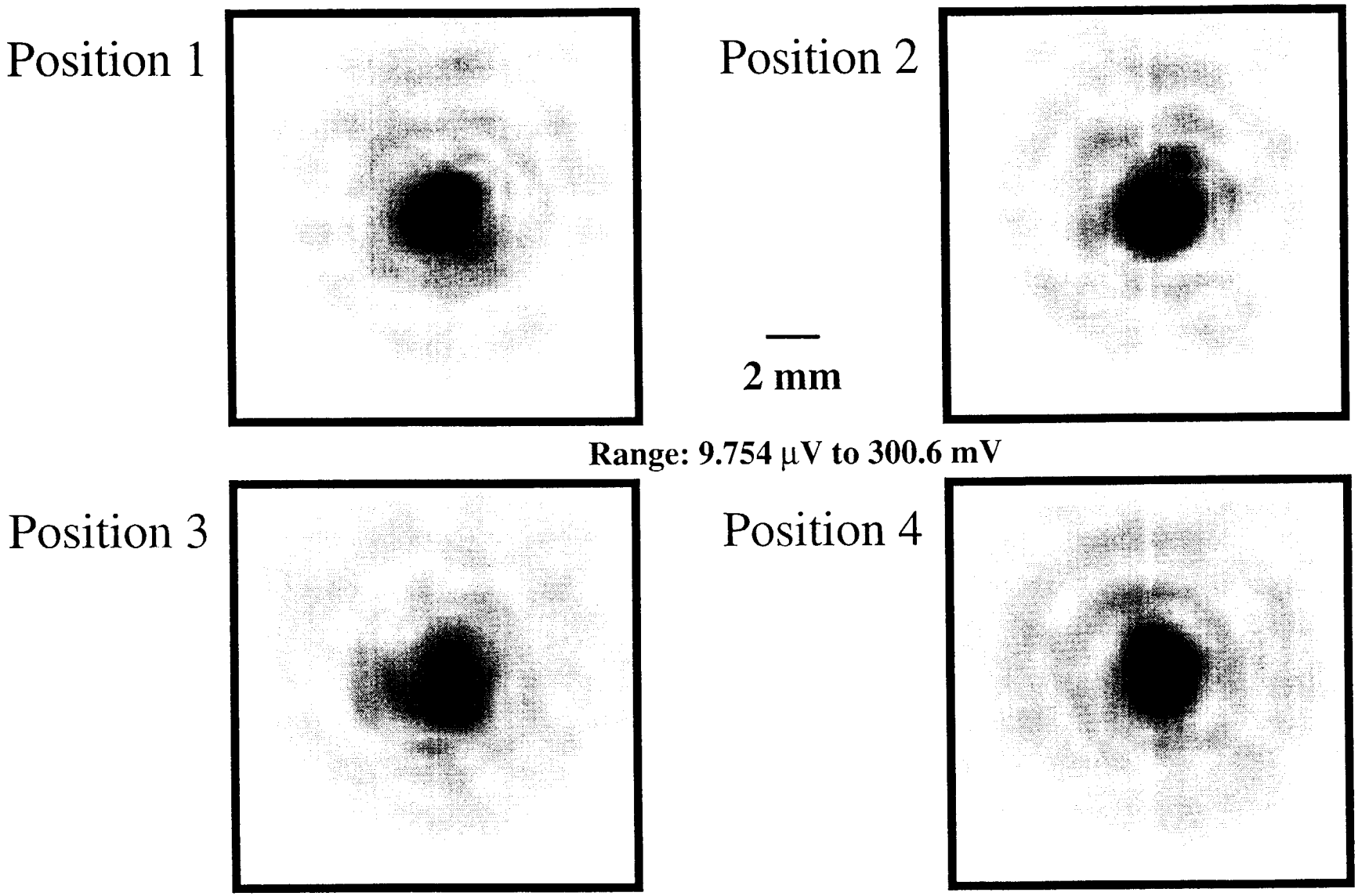

Figure 15: Comparison of positions for 6.5 MHz to 7.5 MHz. Receiver plane images of the narrowband pressure magnitude are shown for the different scanned regions of the thin composite using the 5 MHz transducer.

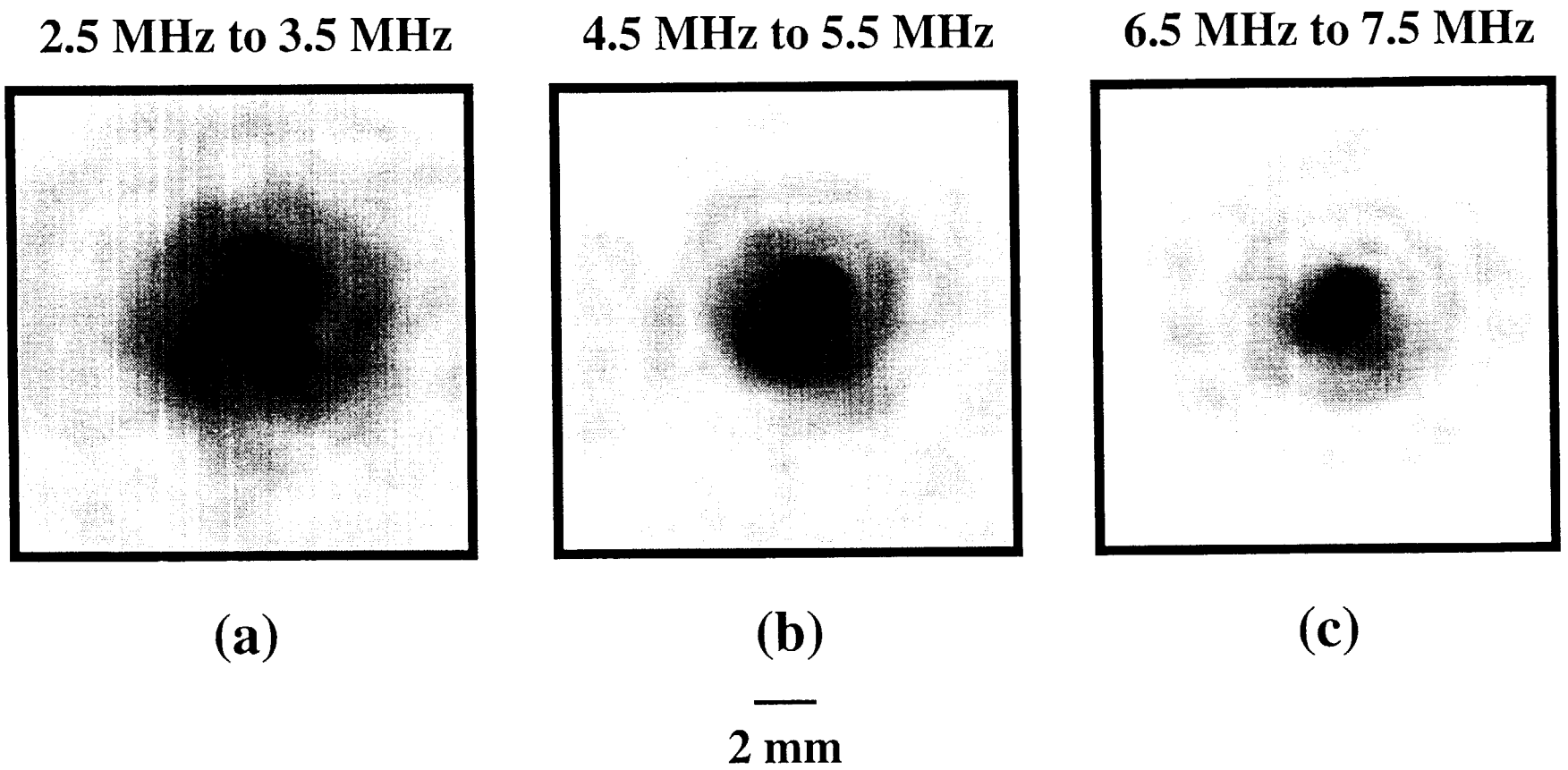

Figure 16: Comparison of insonifying frequencies at Position 1 with 5 MHz transducer. Receiver plane images of the narrowband pressure magnitudes at Position 1 of the thin composite are shown for the different frequency ranges for the 5 MHz transducer.

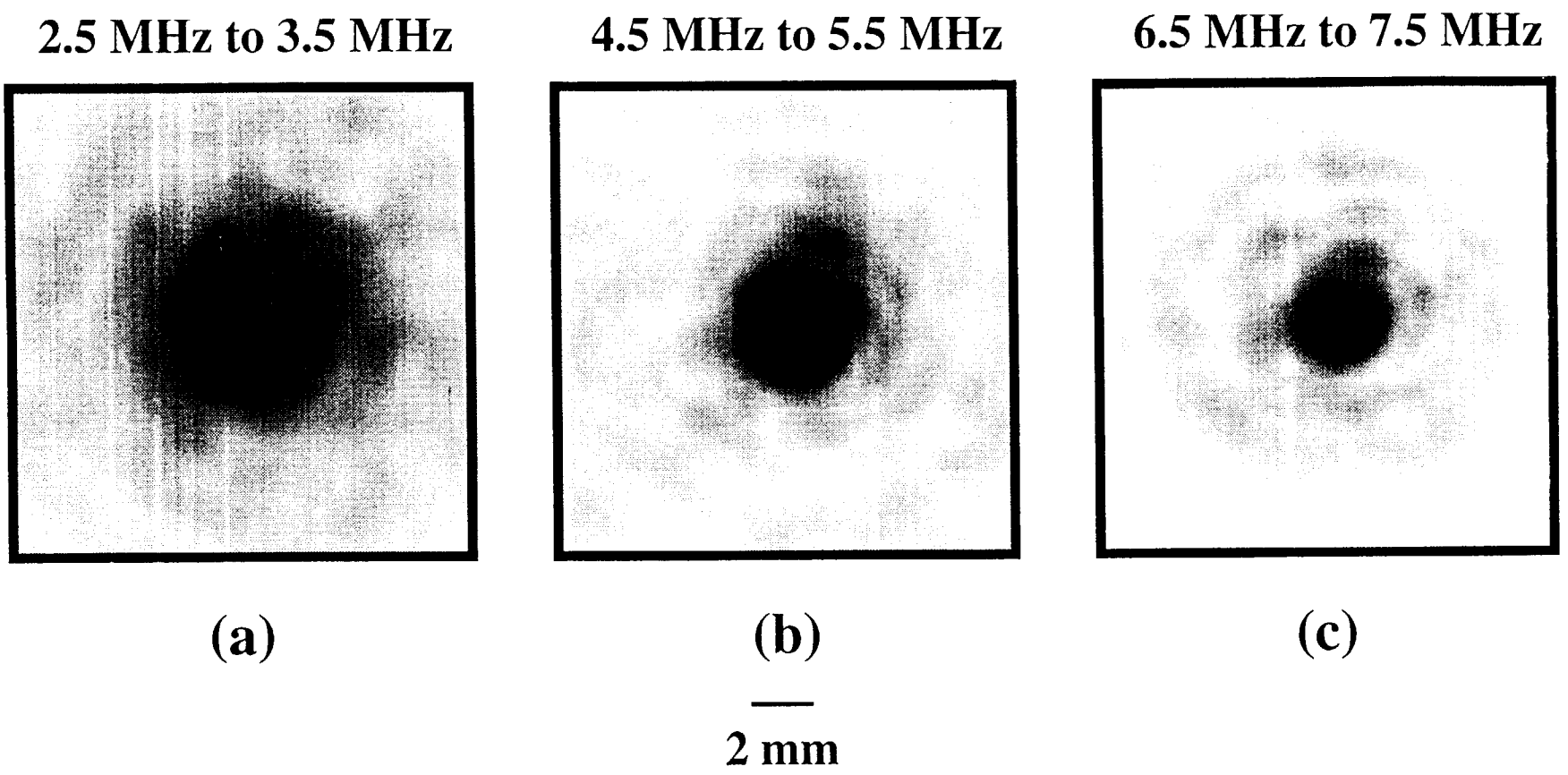

Figure 17: Comparison of insonifying frequencies at Position 2 with 5 MHz transducer. Receiver plane images of the narrowband pressure magnitudes at Position 2 of the thin composite are shown for the different frequency ranges for the 5 MHz transducer.

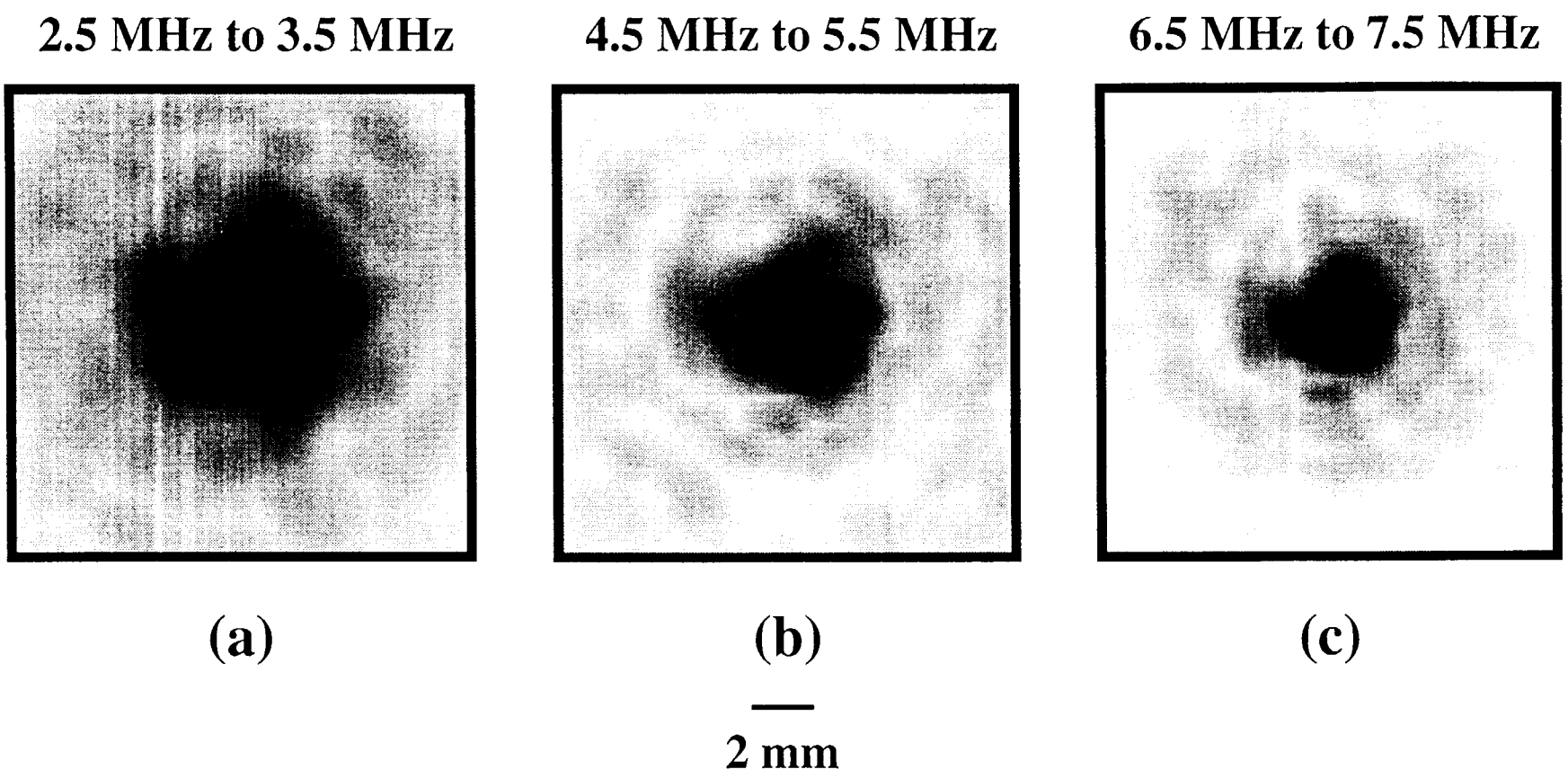

Figure 18: Comparison of insonifying frequencies at Position 3 with 5 MHz transducer. Receiver plane images of the narrowband pressure magnitudes at Position 3 of the thin composite are shown for the different frequency ranges for the 5 MHz transducer.

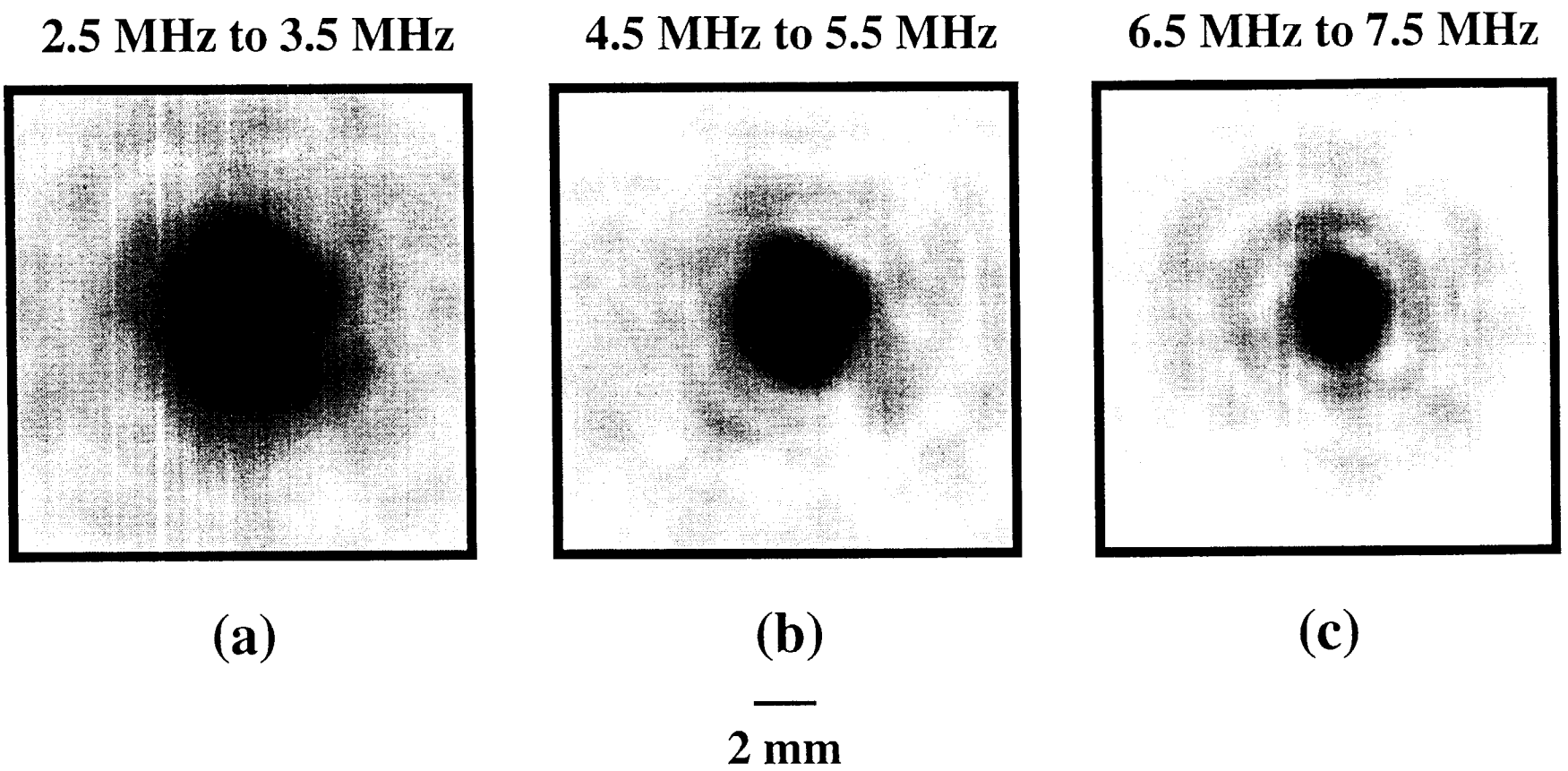

Figure 19: Comparison of insonifying frequencies at Position 4 with 5 MHz transducer. Receiver plane images of the narrowband pressure magnitudes at Position 4 of the thin composite are shown for the different frequency ranges for the 5 MHz transducer.

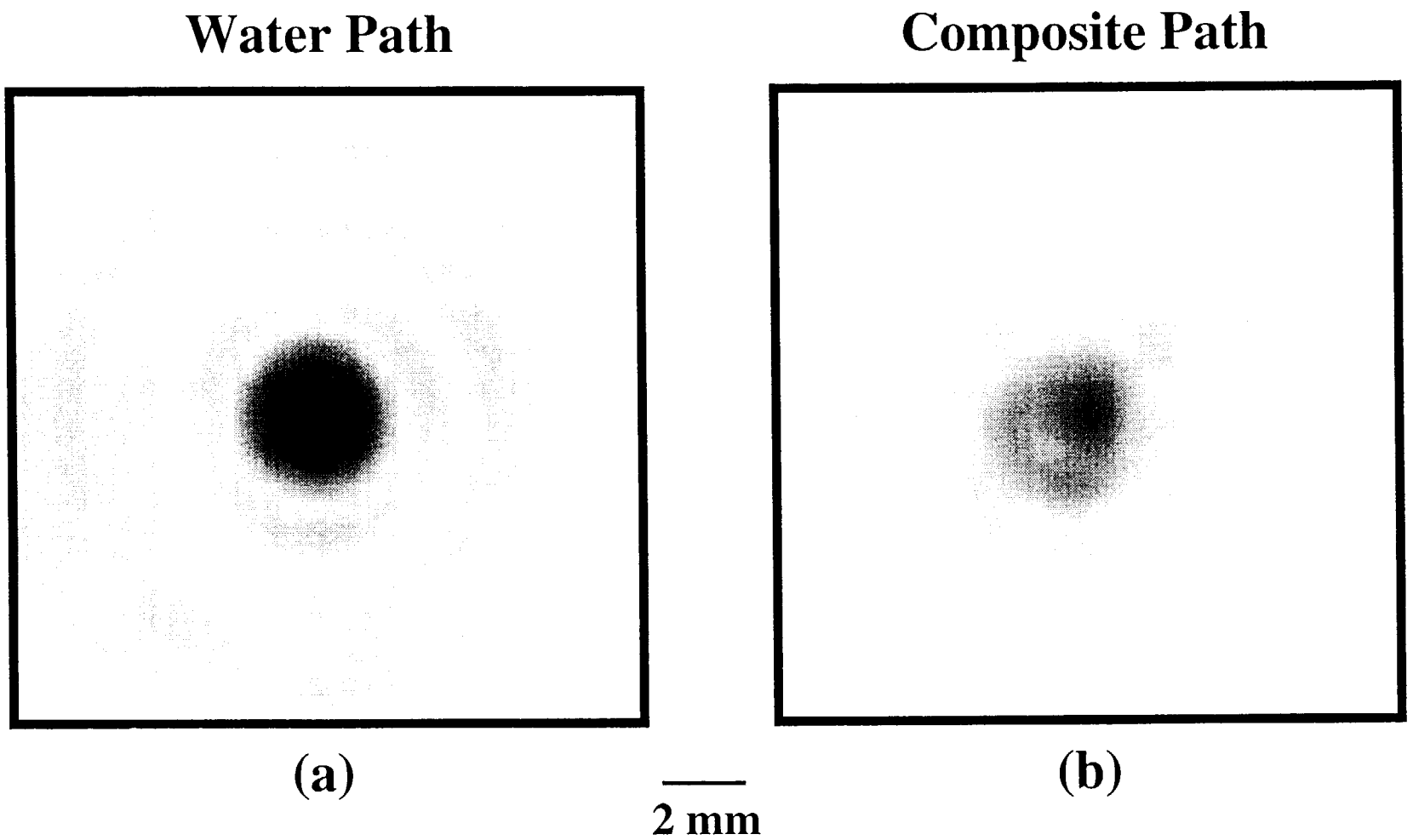

Figure 20: Water path versus composite path for 7.5 MHz to 8.5 MHz. Receiver plane images for (a) narrowband pressure magnitude for water path only and (b) narrowband pressure magnitude for composite path using the 10 MHz transducer.

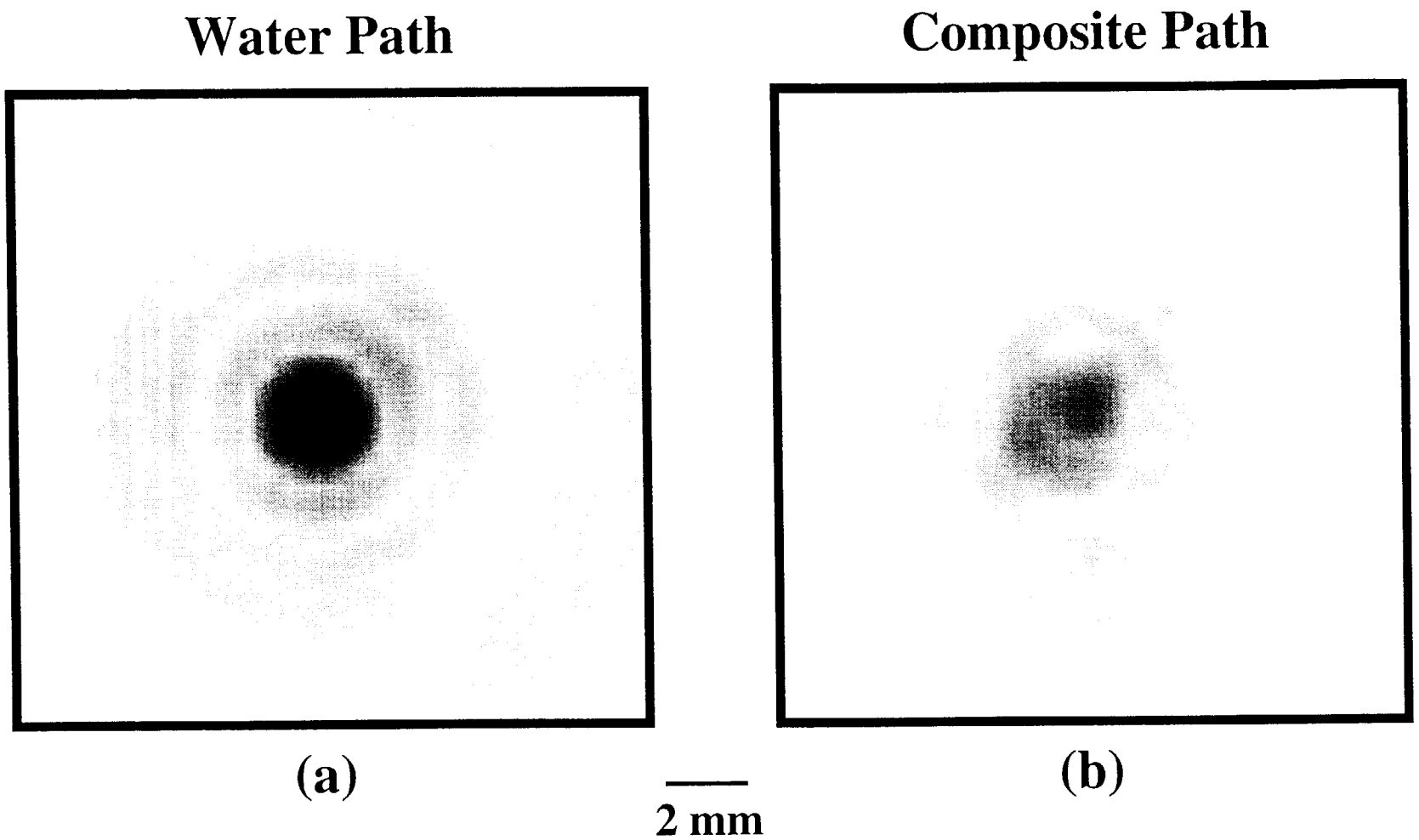

Figure 21: Water path versus composite path for 9.5 MHz to 10.5 MHz. Receiver plane images for (a) narrowband pressure magnitude for water path only and (b) narrowband pressure magnitude for composite path using the 10 MHz transducer.

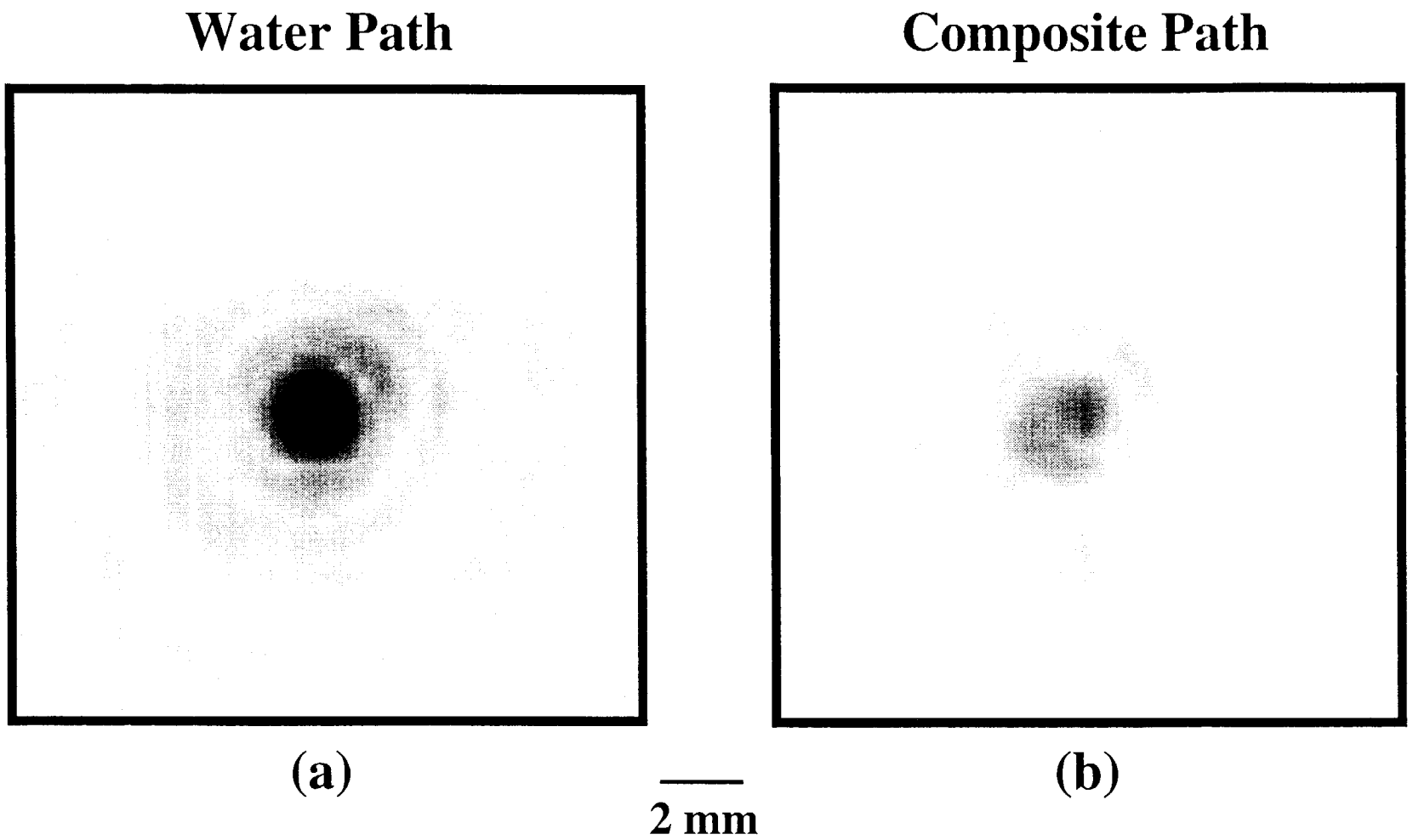

Figure 22: Water path versus composite path for 11.5 MHz to 12.5 MHz. Receiver plane images for (a) narrowband pressure magnitude for water path only and (b) narrowband pressure magnitude for composite path using the 10 MHz transducer.

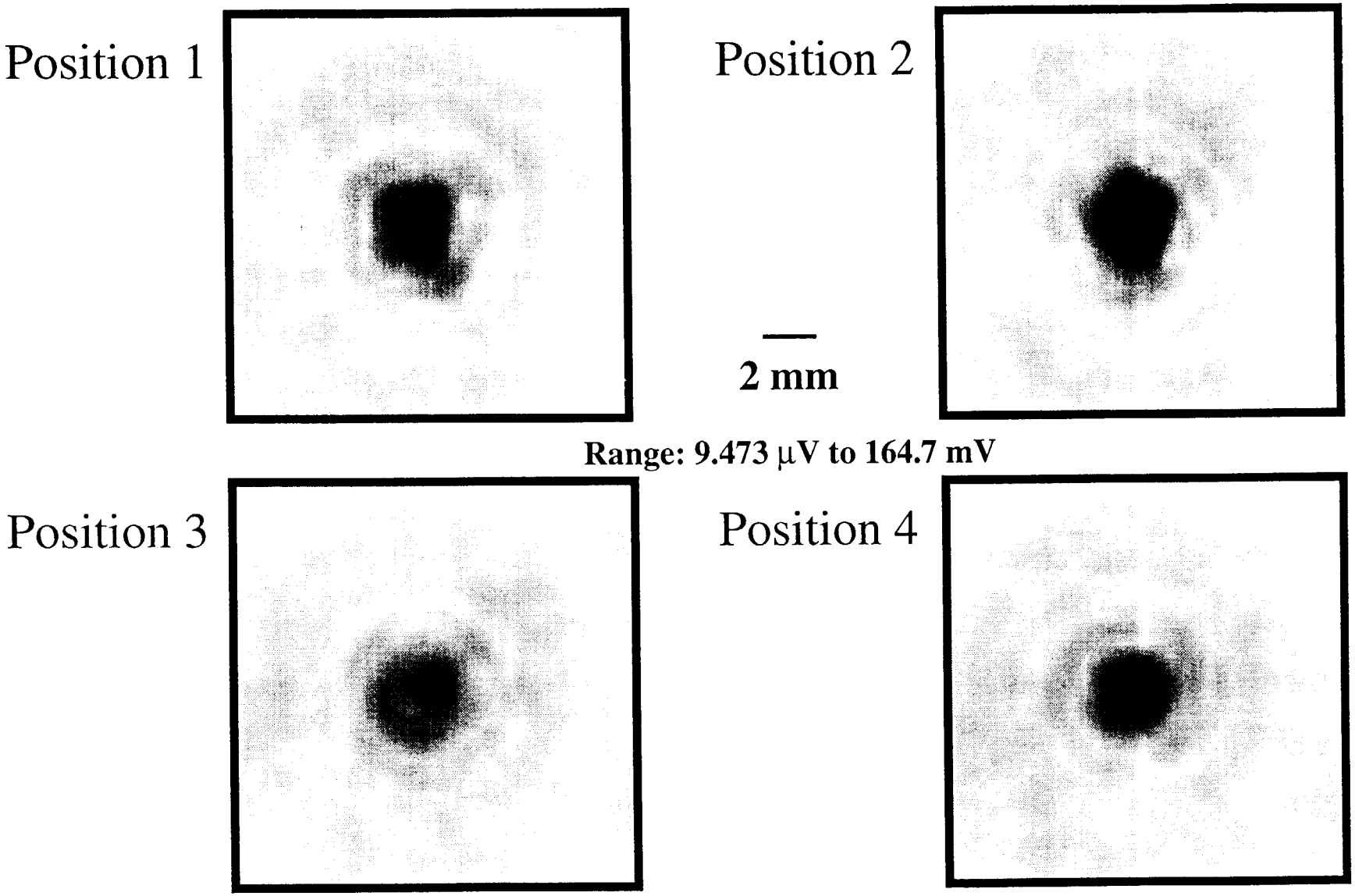

Figure 23: Comparison of positions for 7.5 MHz to 8.5 MHz. Receiver plane images of the narrowband pressure magnitude are shown for the different scanned regions of the thin composite using the 10 MHz transducer.

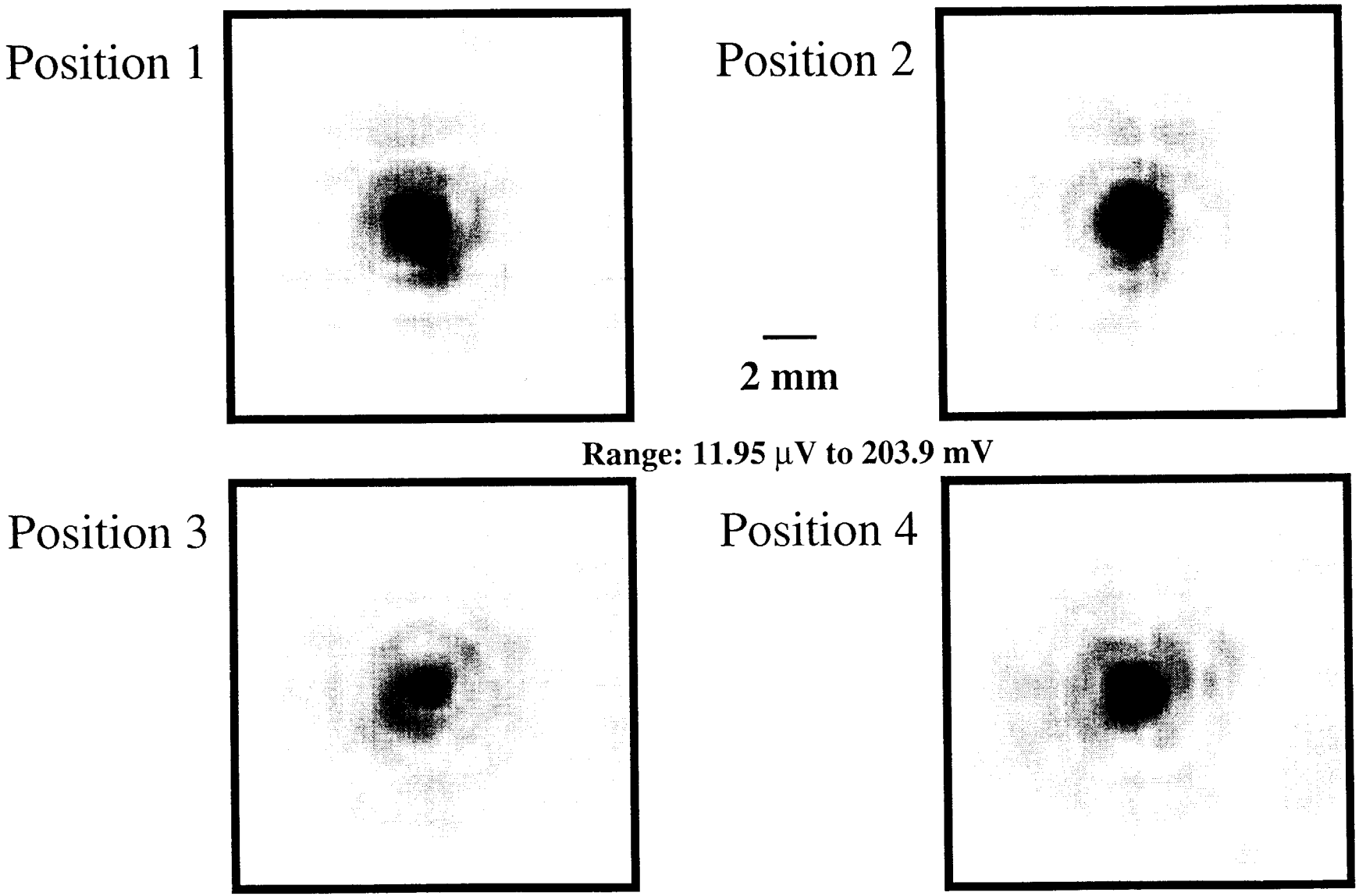

Figure 24: Comparison of positions for 9.5 MHz to 10.5 MHz. Receiver plane images of the narrowband pressure magnitude are shown for the different scanned regions of the thin composite using the 10 MHz transducer.

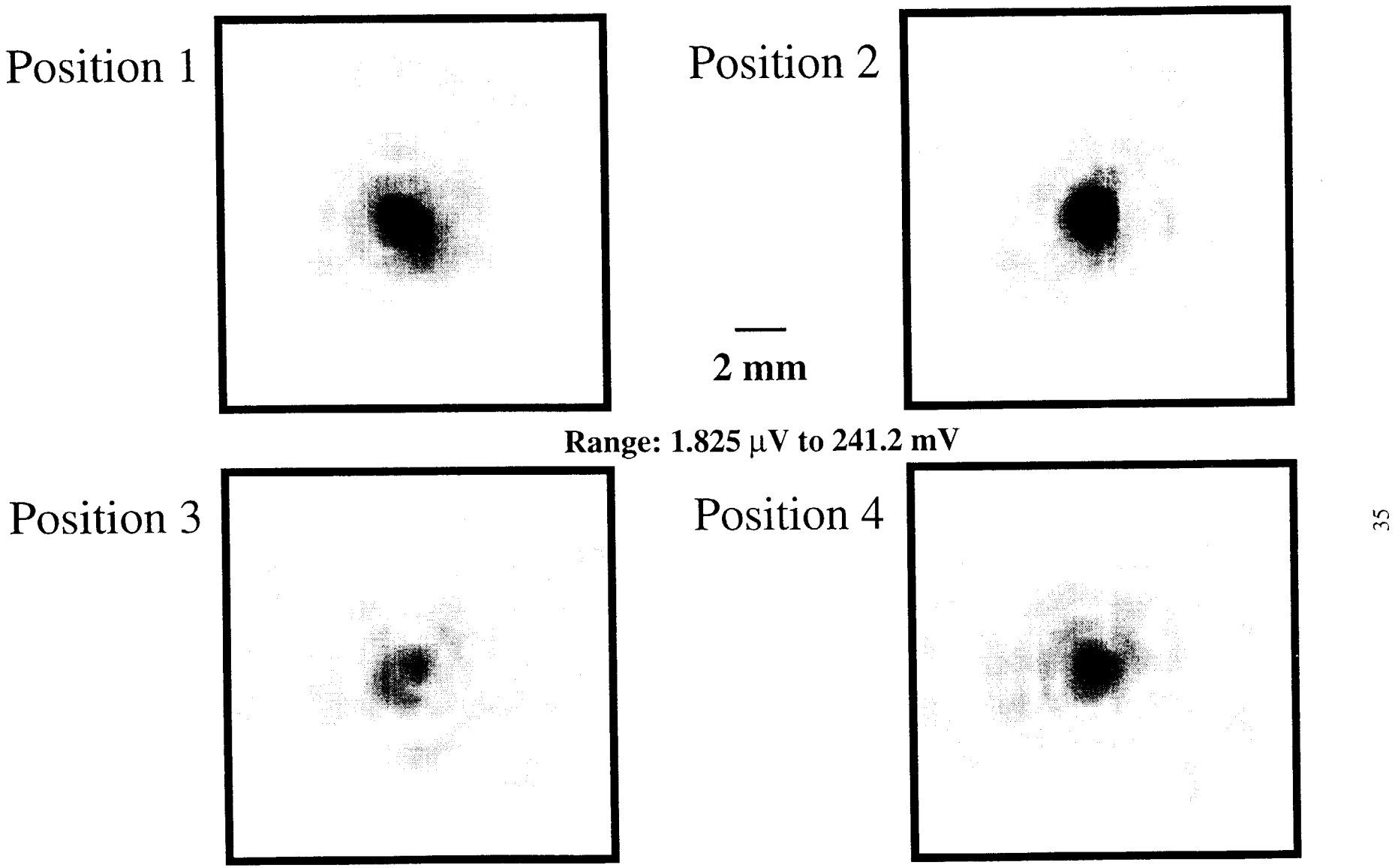

Figure 25: Comparison of positions for 11.5 MHz to 12.5 MHz. Receiver plane images of the narrowband pressure magnitude are shown for the different scanned regions of the thin composite using the 10 MHz transducer.

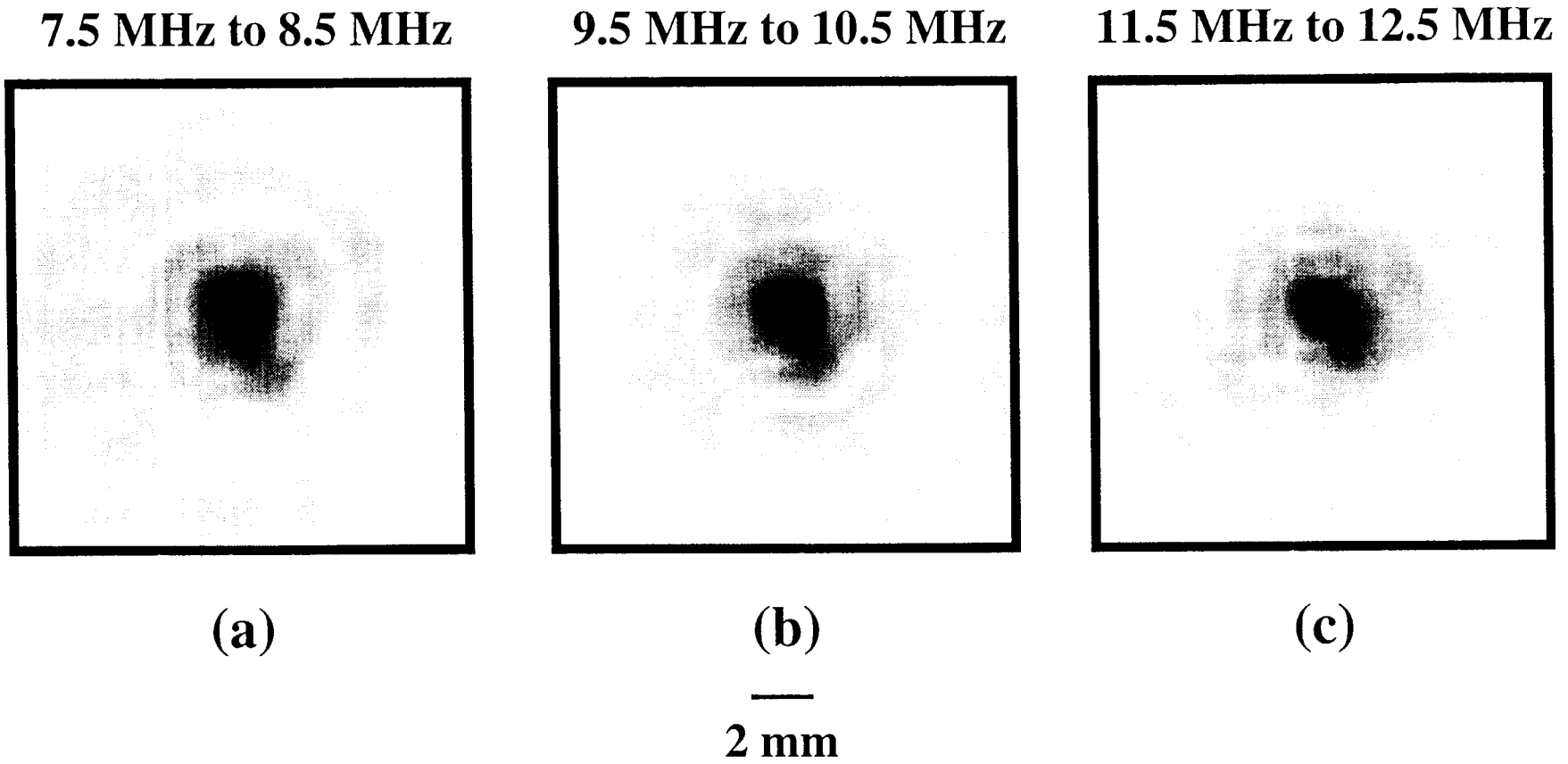

Figure 26: Comparison of insonifying frequencies at Position 1 with 10 MHz transducer. Receiver plane images of the narrowband pressure magnitudes at Position 1 of the thin composite are shown for the different frequency ranges for the 10 MHz transducer.

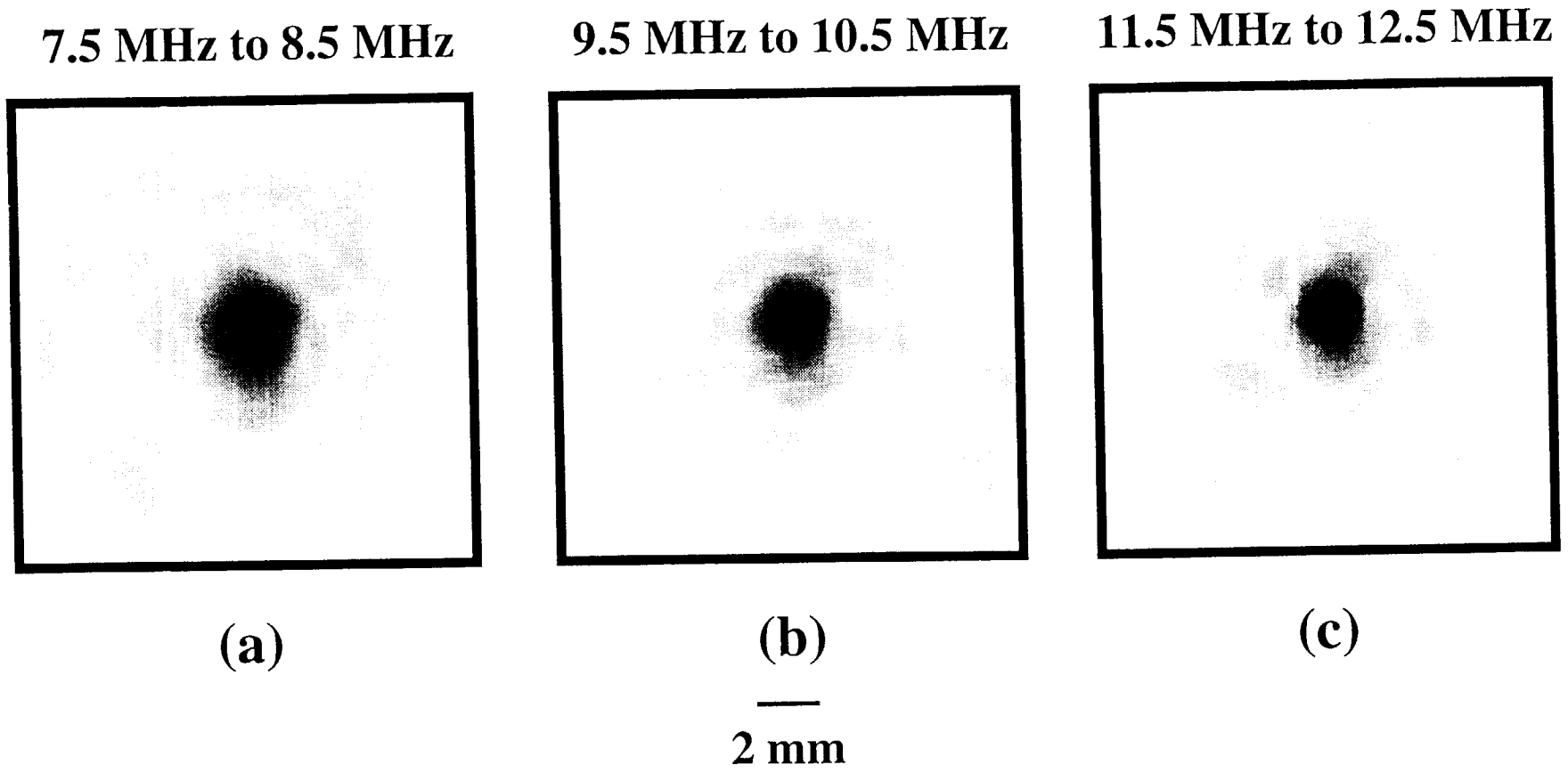

Figure 27: Comparison of insonifying frequencies at Position 2 with 10 MHz transducer. Receiver plane images of the narrowband pressure magnitudes at Position 2 of the thin composite are shown for the different frequency ranges for the 10 MHz transducer.

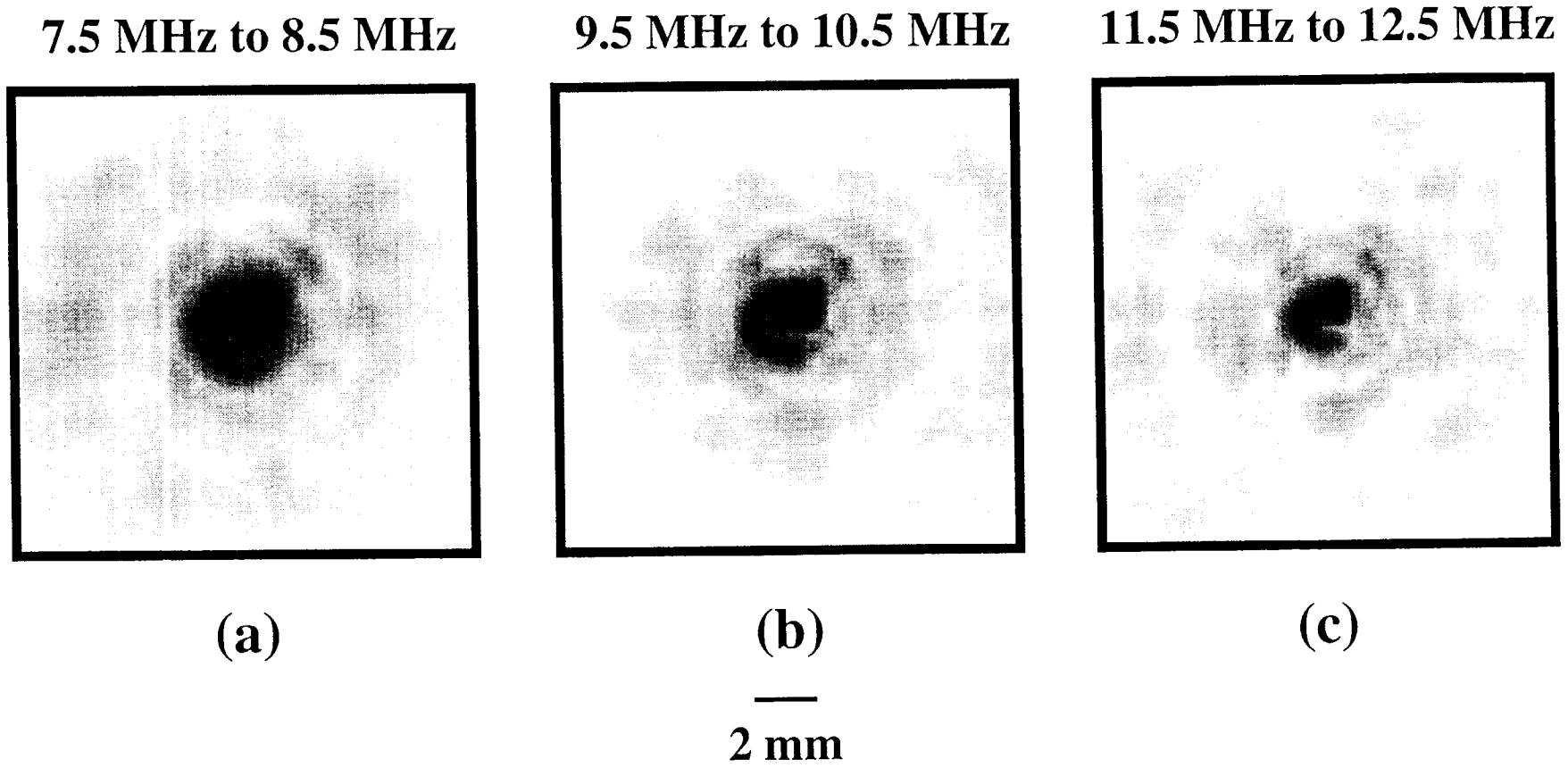

Figure 28: Comparison of insonifying frequencies at Position 3 with 10 MHz transducer. Receiver plane images of the narrowband pressure magnitudes at Position 3 of the thin composite are shown for the different frequency ranges for the 10 MHz transducer.

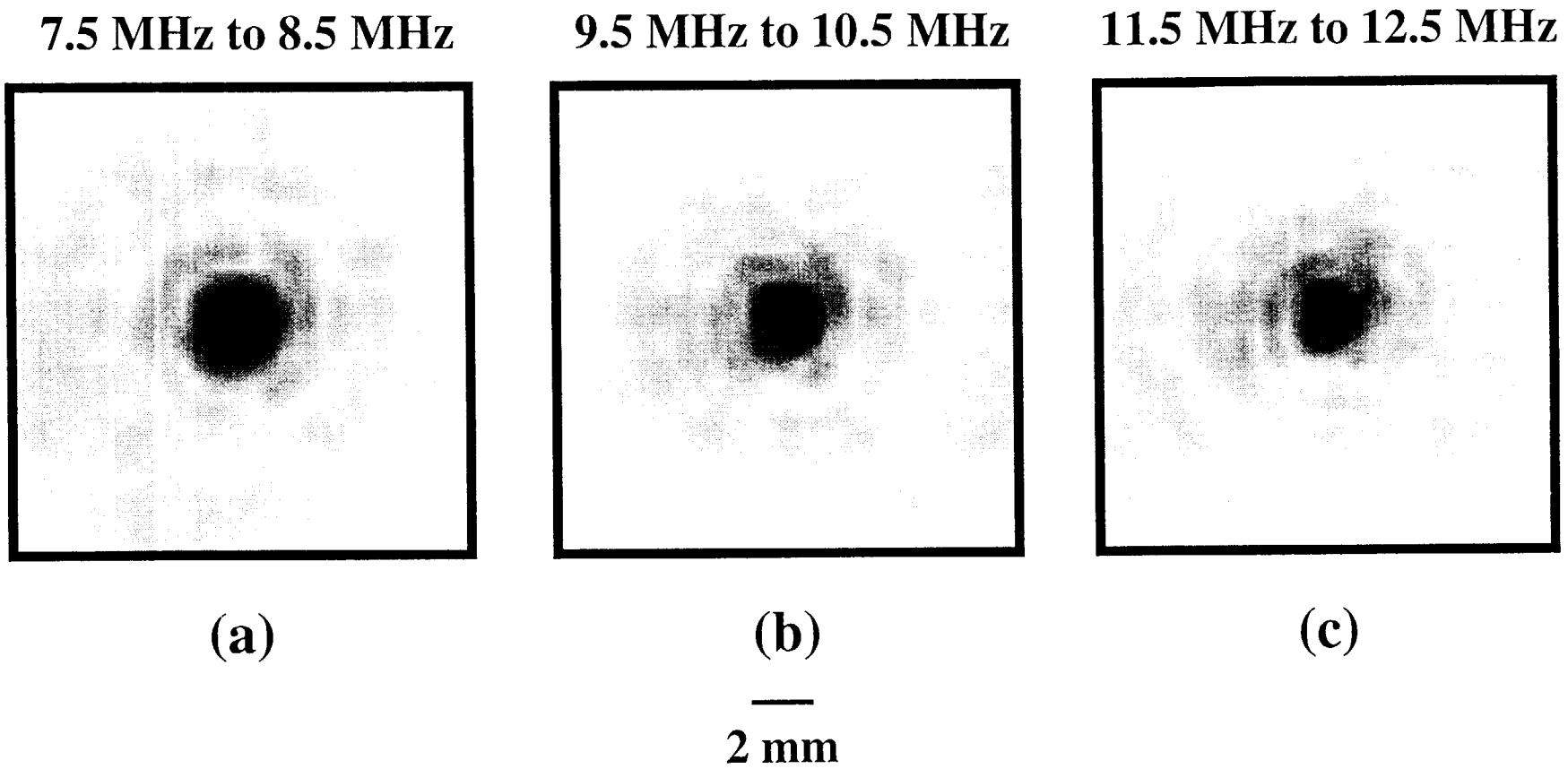

Figure 29: Comparison of insonifying frequencies at Position 4 with 10 MHz transducer. Receiver plane images of the narrowband pressure magnitudes at Position 4 of the thin composite are shown for the different frequency ranges for the 10 MHz transducer.

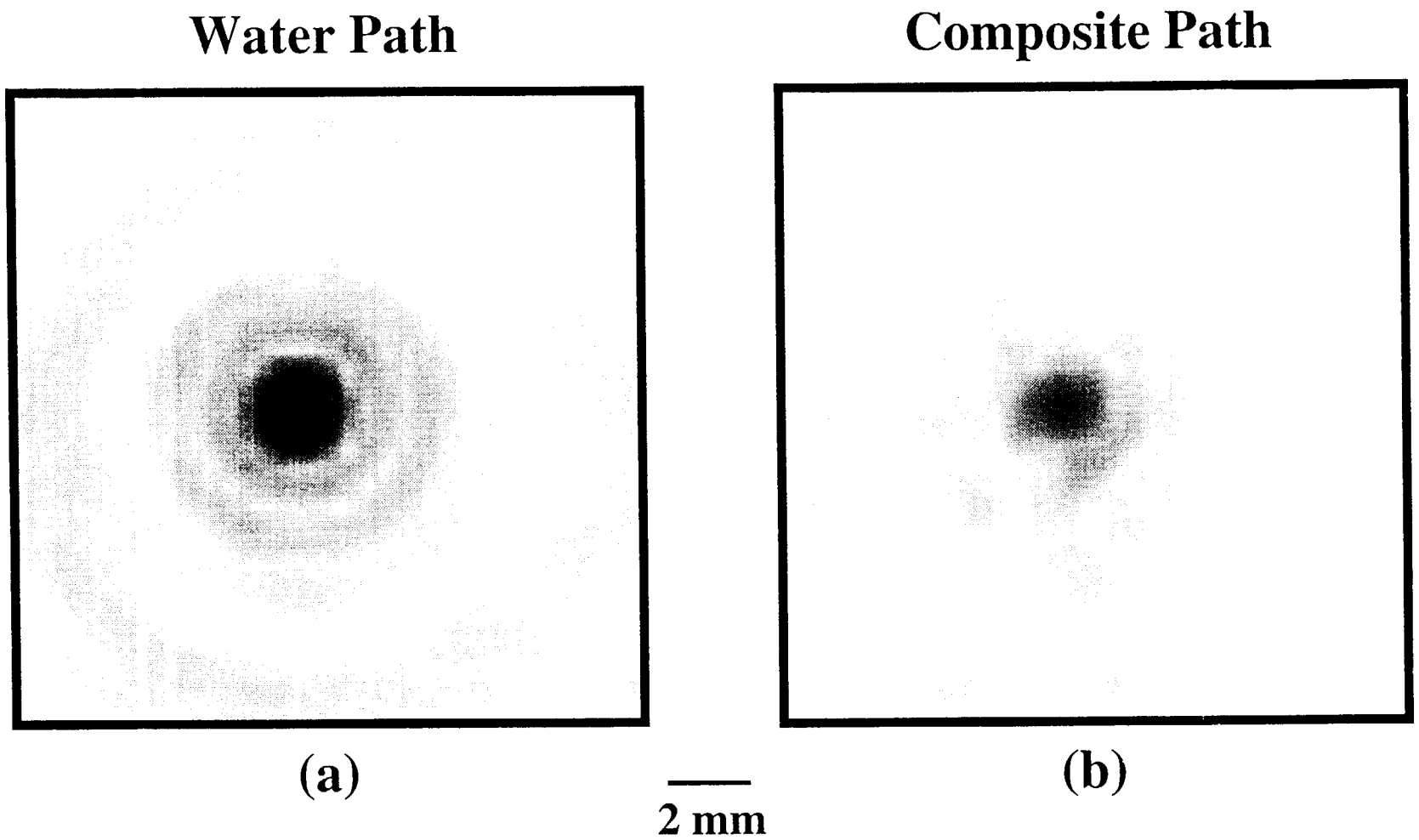

Figure 30: Water path versus composite path for 10.5 MHz to 11.5 MHz. Receiver plane images for (a) narrowband pressure magnitude for water path only and (b) narrowband pressure magnitude for composite path using the 15 MHz transducer.

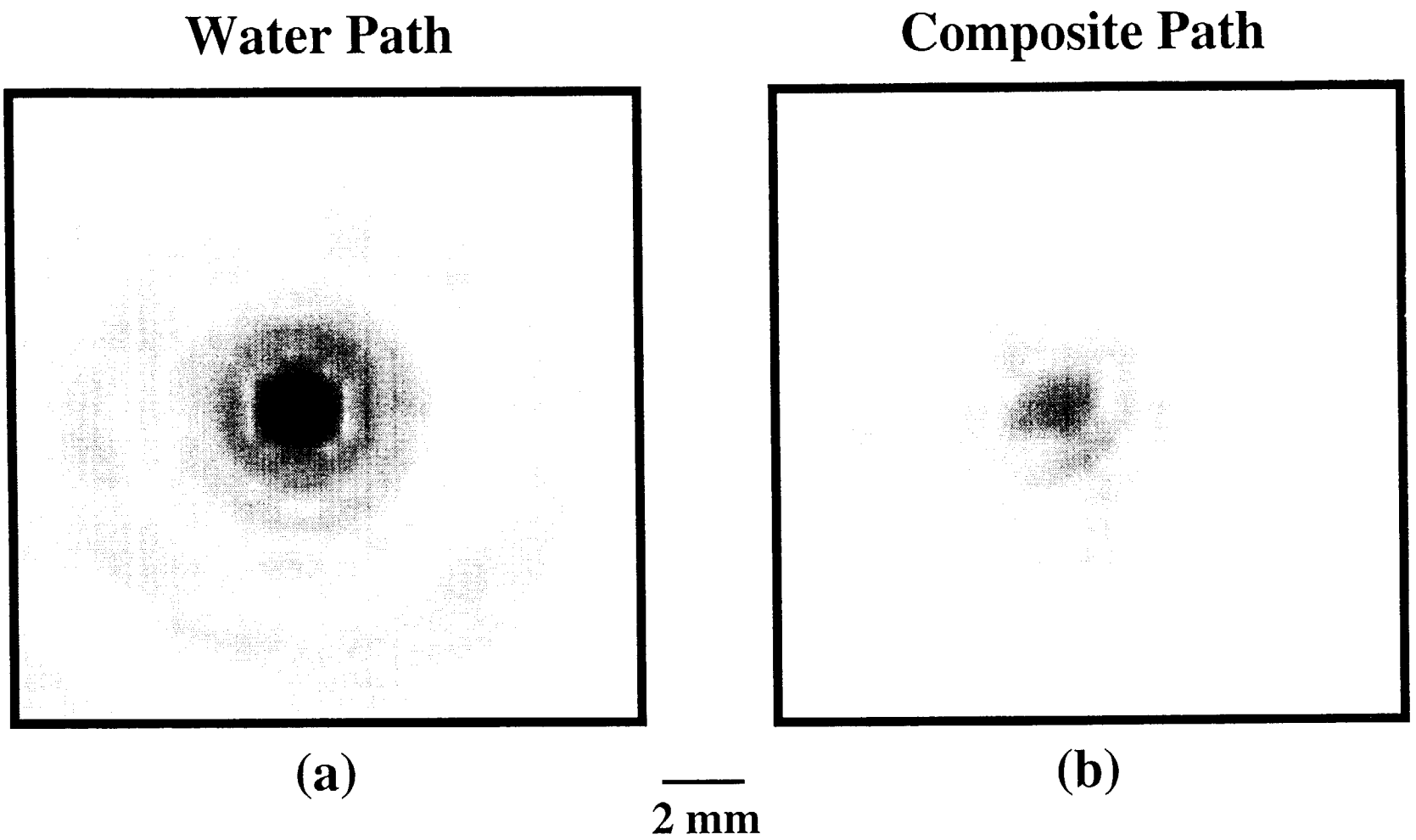

Figure 31: Water path versus composite path for 12.5 MHz to 13.5 MHz. Receiver plane images for (a) narrowband pressure magnitude for water path only and (b) narrowband pressure magnitude for composite path using the 15 MHz transducer.

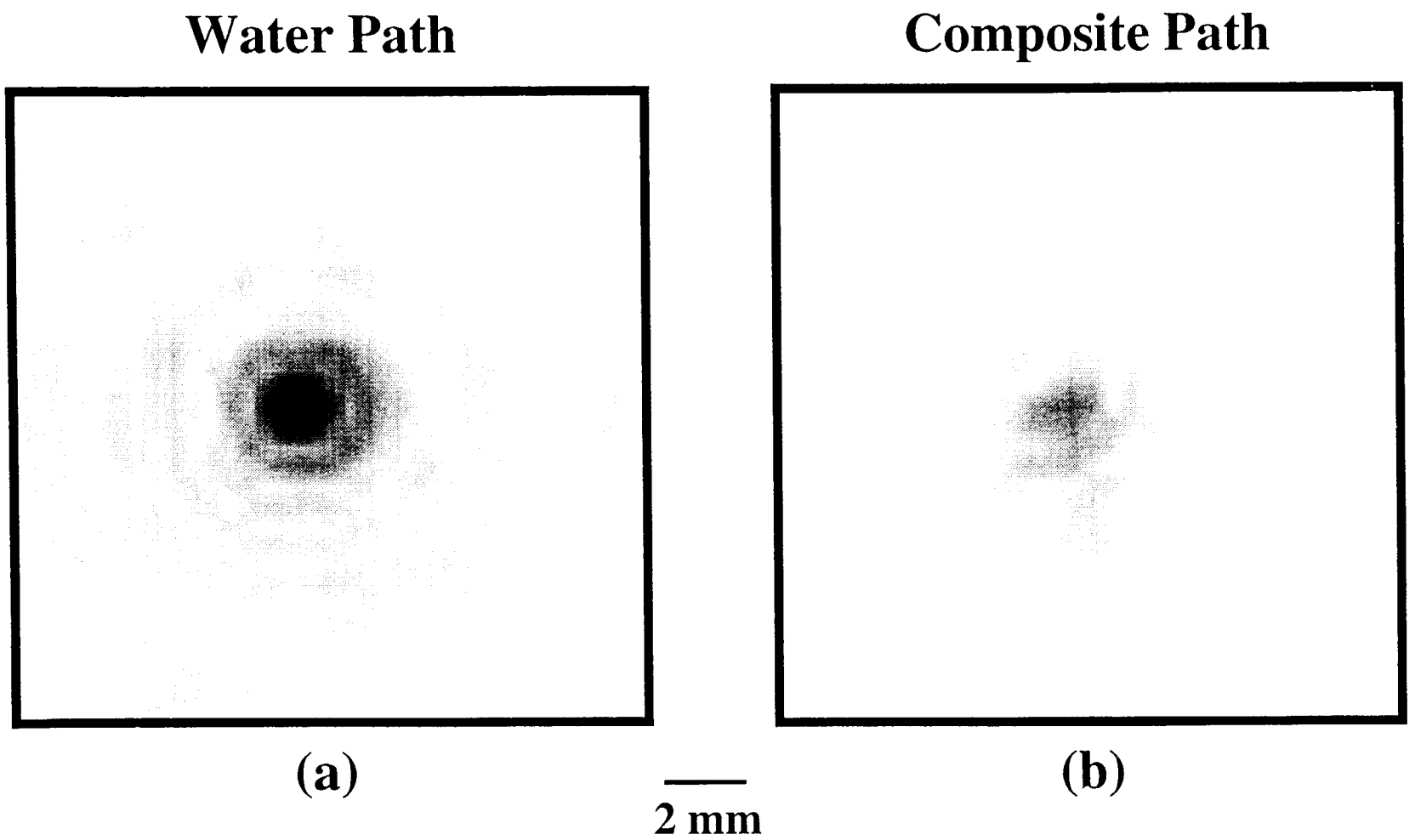

Figure 32: Water path versus composite path for 14.5 MHz to 15.5 MHz. Receiver plane images for (a) narrowband pressure magnitude for water path only and (b) narrowband pressure magnitude for composite path using the 15 MHz transducer.

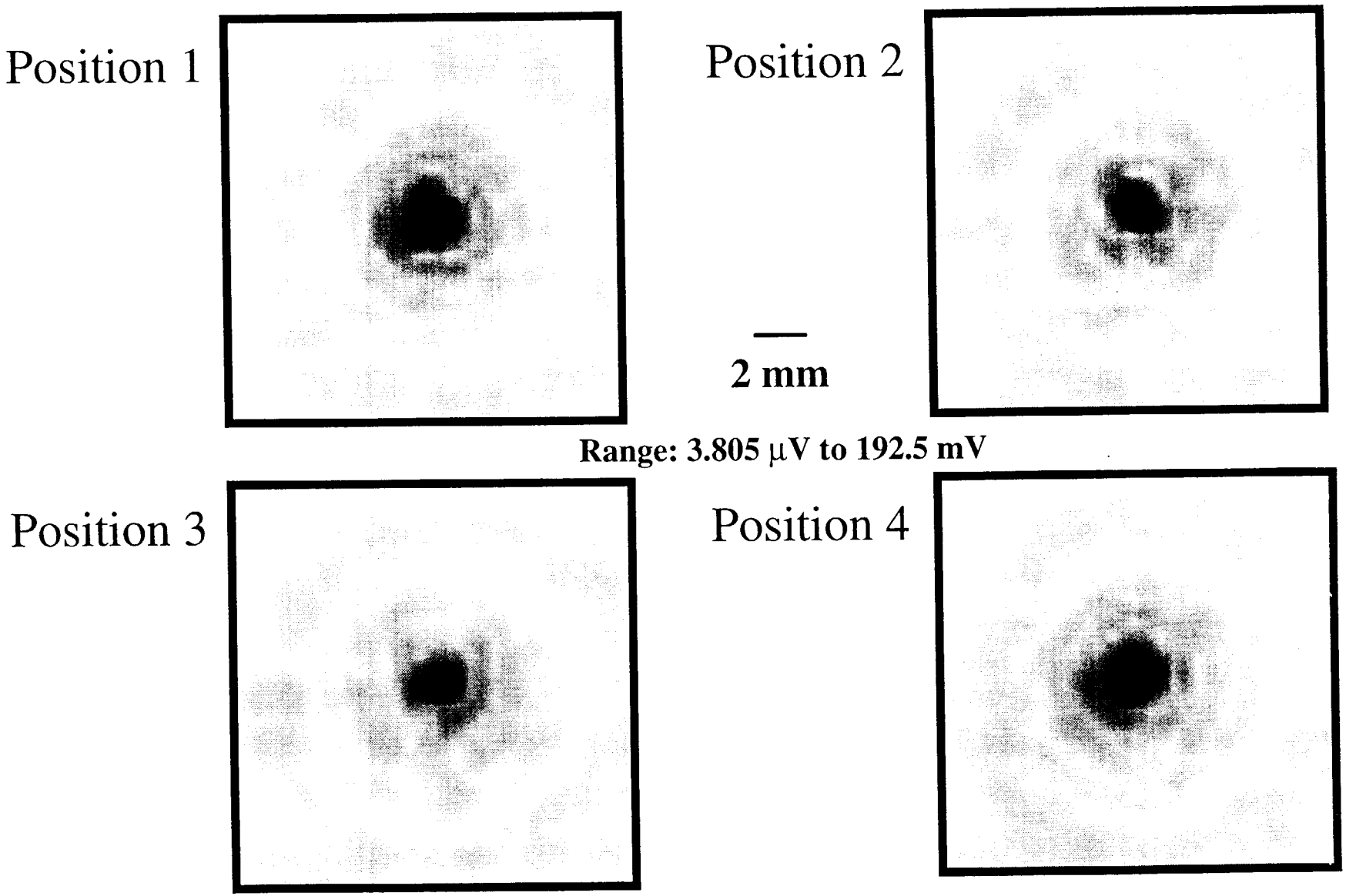

Figure 33: Comparison of positions for 10.5 MHz to 11.5 MHz. Receiver plane images of the narrowband pressure magnitude are shown for the different scanned regions of the thin composite using the 15 MHz transducer.

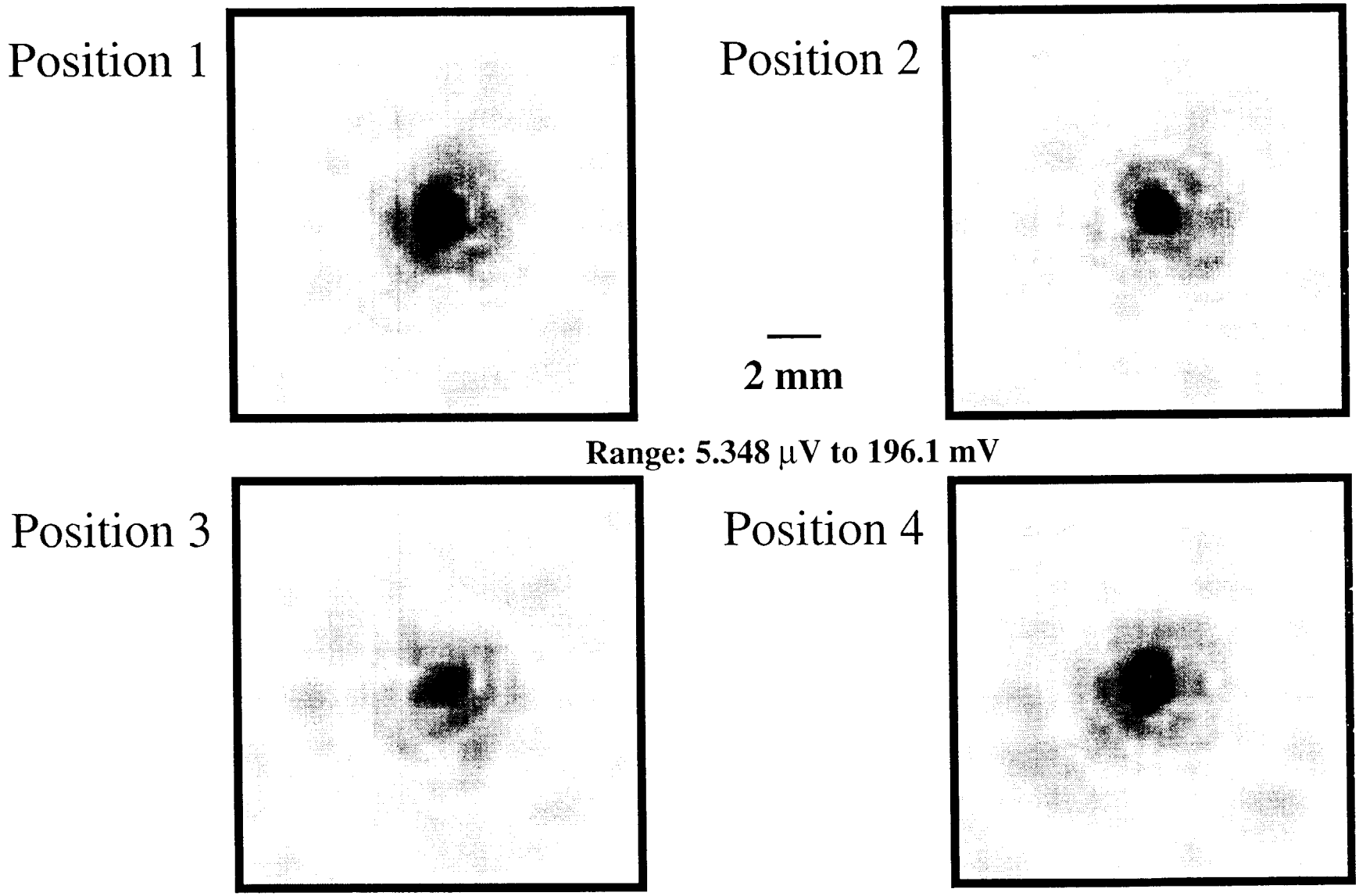

Figure 34: Comparison of positions for 12.5 MHz to 13.5 MHz. Receiver plane images of the narrowband pressure magnitude are shown for the different scanned regions of the thin composite using the 15 MHz transducer.

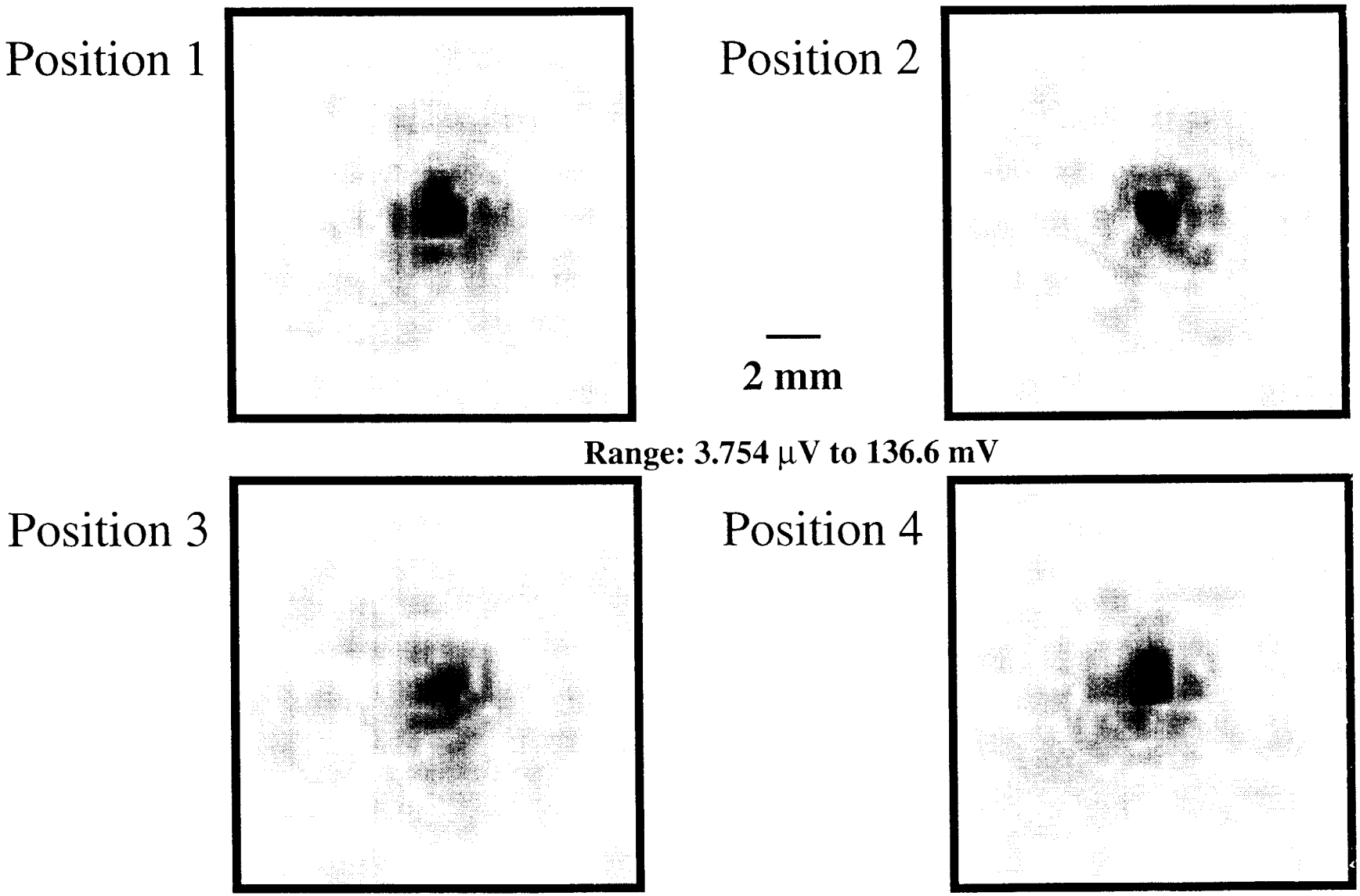

Figure 35: Comparison of positions for 14.5 MHz to 15.5 MHz. Receiver plane images of the narrowband pressure magnitude are shown for the different scanned regions of the thin composite using the 15 MHz transducer.

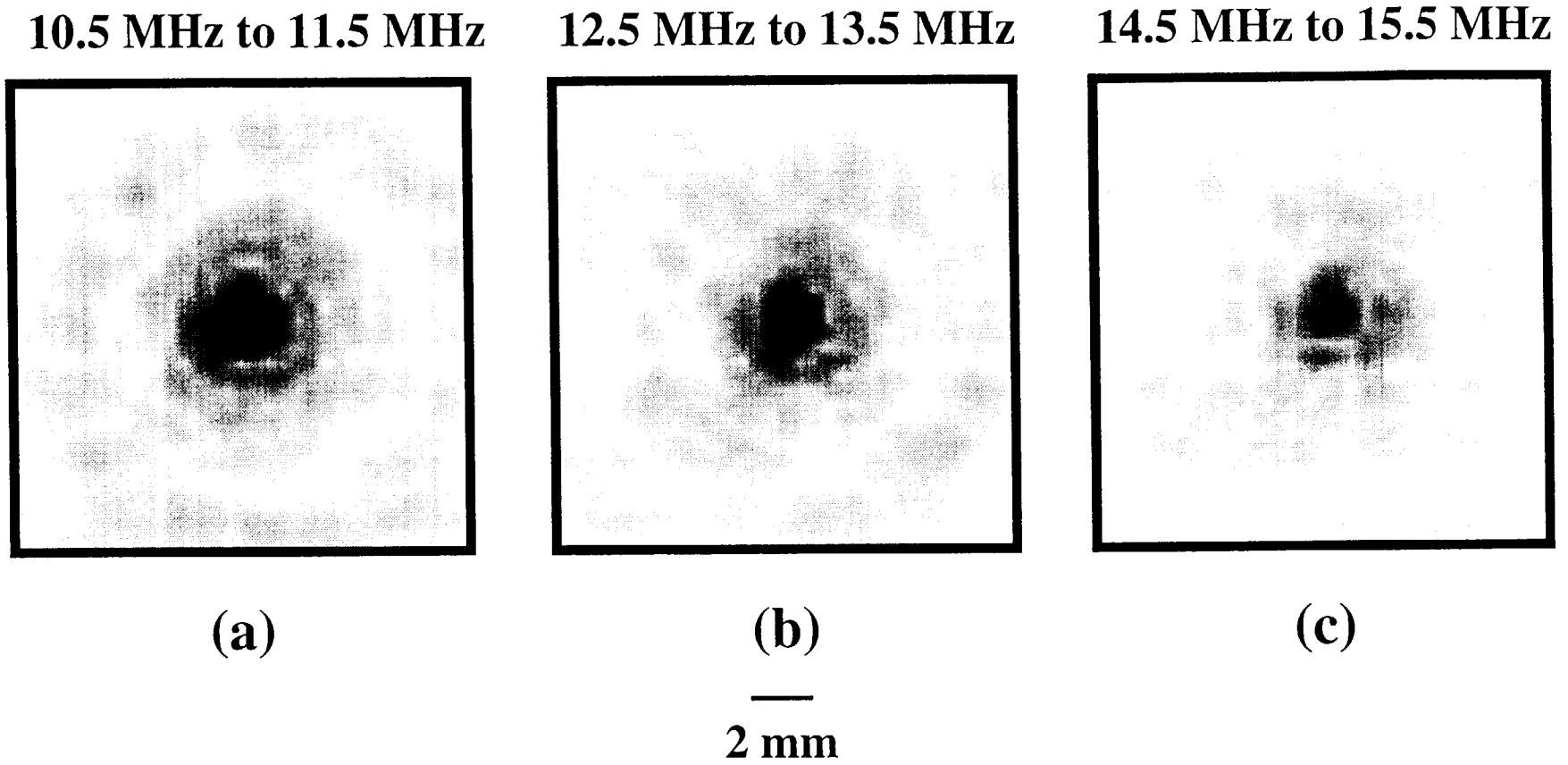

Figure 36: Comparison of insonifying frequencies at Position 1 with 15 MHz transducer. Receiver plane images of the narrowband pressure magnitudes at Position 1 of the thin composite are shown for the different frequency ranges for the 15 MHz transducer.

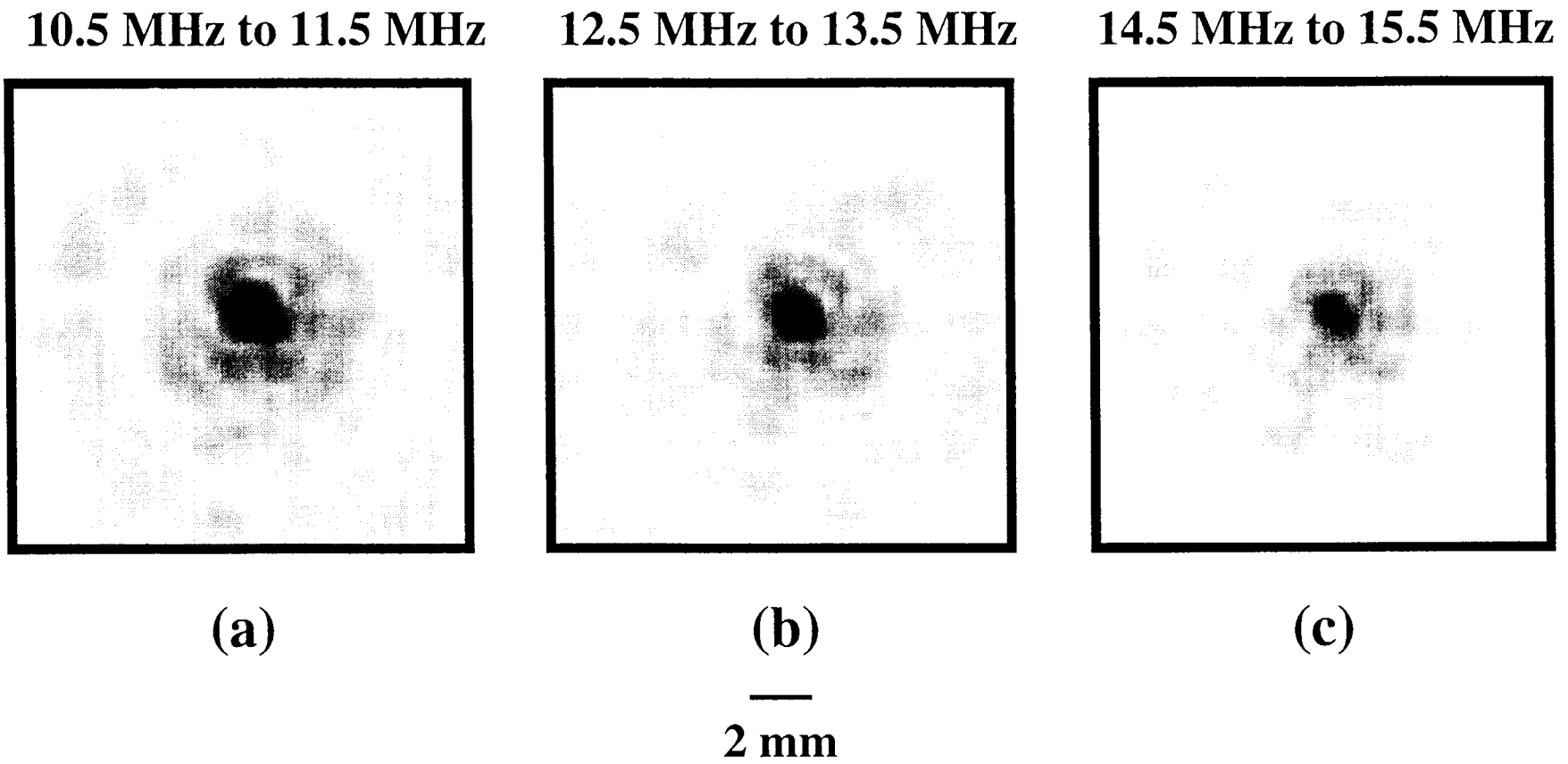

Figure 37: Comparison of insonifying frequencies at Position 2 with 15 MHz transducer. Receiver plane images of the narrowband pressure magnitudes at Position 2 of the thin composite are shown for the different frequency ranges for the 15 MHz transducer.

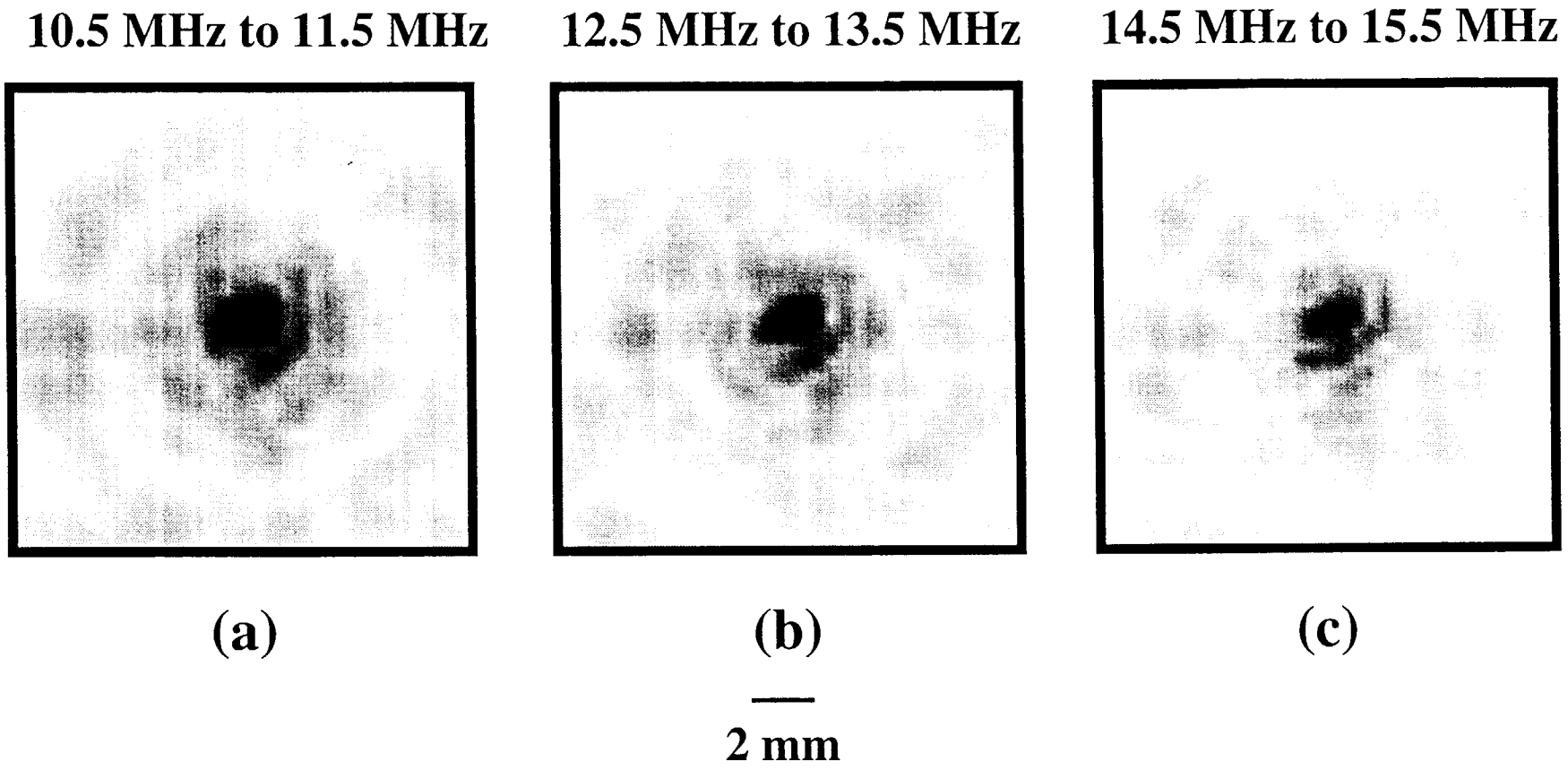

Figure 38: Comparison of insonifying frequencies at Position 3 with 15 MHz transducer. Receiver plane images of the narrowband pressure magnitudes at Position 3 of the thin composite are shown for the different frequency ranges for the 15 MHz transducer.

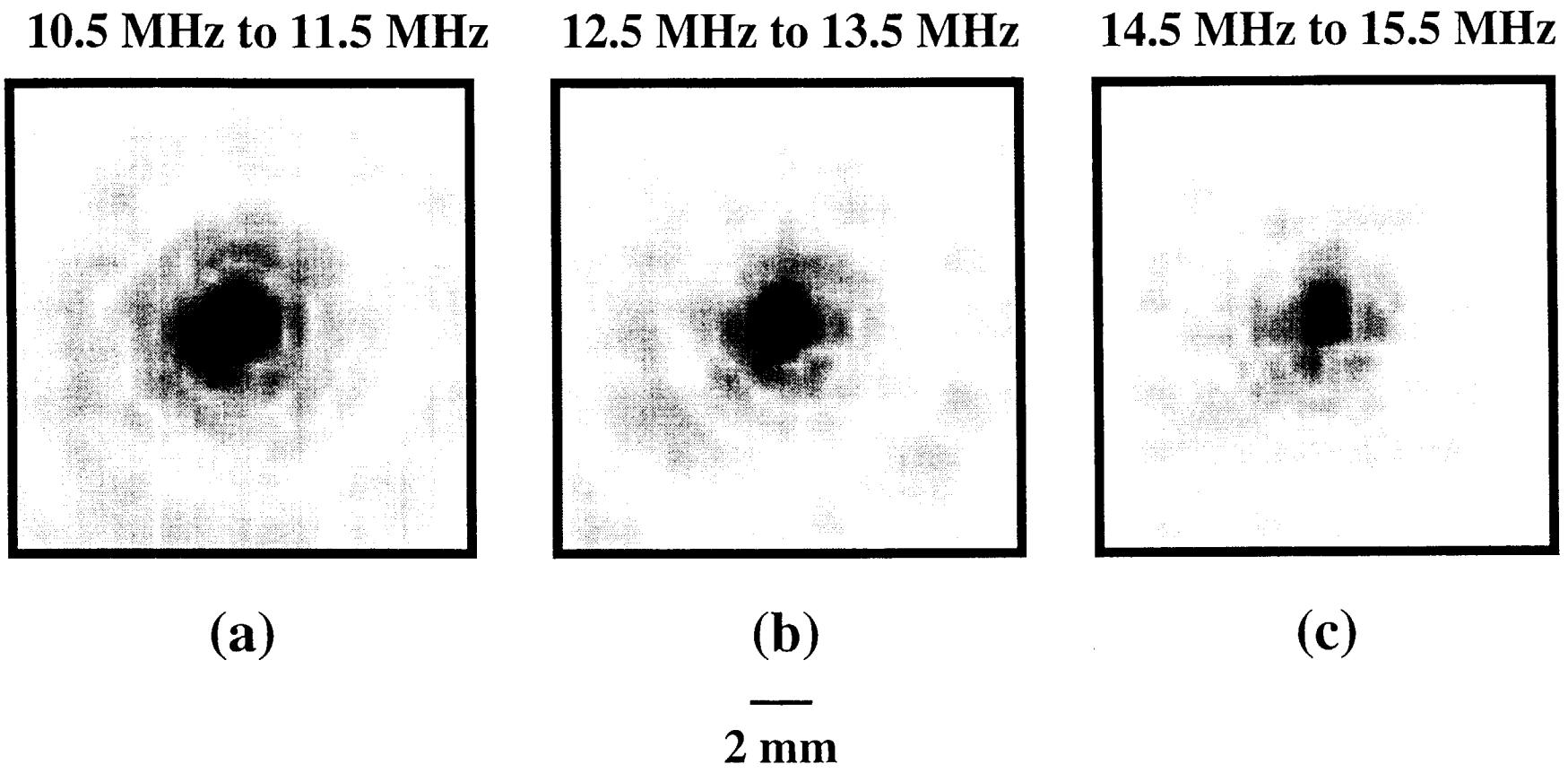

Figure 39: Comparison of insonifying frequencies at Position 4 with 15 MHz transducer. Receiver plane images of the narrowband pressure magnitudes at Position 4 of the thin composite are shown for the different frequency ranges for the 15 MHz transducer.

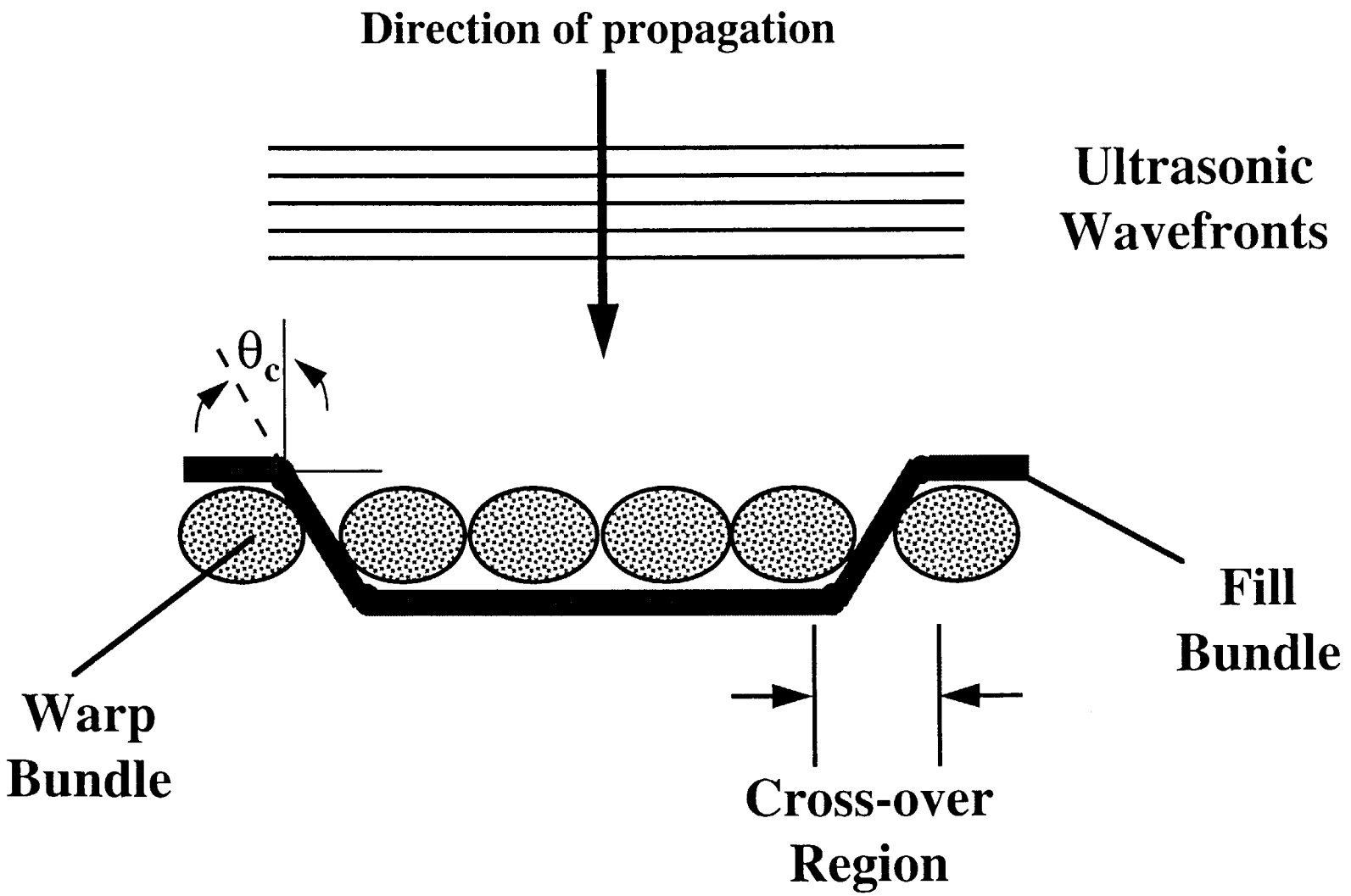

Figure 40: Cartoon of a sideview of the thin woven composite. The composite is shown in relation to an impinging ultrasonic pressure field. Note the direction of propagation of the ultrasonic wavefronts are normal with respect to the warp orientation and the ultrasonic wavefronts are at an angle θ_c with respect to the fill orientation.

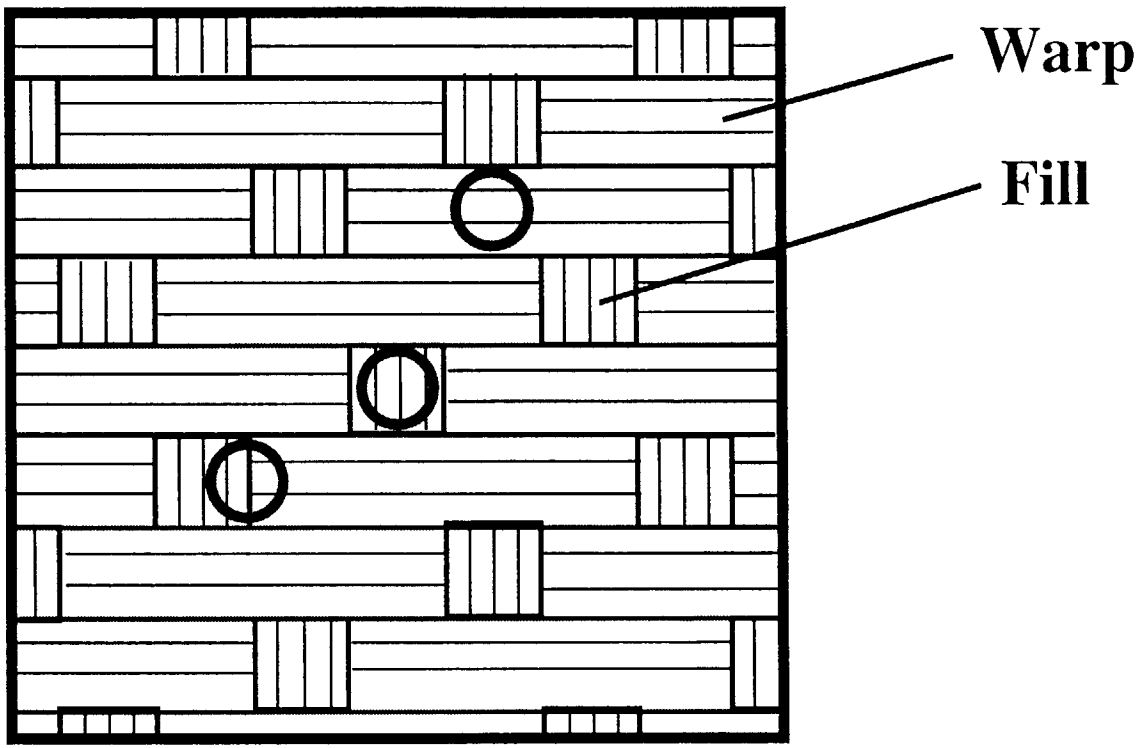

Figure 41: Cartoon of the front surface of the thin woven composite marked with possible positions of an ultrasonic main beam footprint. The solid-line circles represent ultrasonic beams whose diameters are either contained within the dimensions of a fiber bundle (warp or fill) or overlie the edges of the warp and fill.